Is the Sicily Channel a simple Rifting Zone? New evidence from seismic analysis with geodynamic implications

Mariagiada Maiorana [a,*], Andrea Artoni [b], Eline Le Breton [c], Attilio Sulli [a], Nicolò Chizzini [b], Luigi Torelli [b]

[a] *Department of Earth and Marine Sciences, University of Palermo, Via Archirafi 22, 90123 Palermo, Italy*
[b] *Department of Chemistry, Life Sciences and Environmental Sustainability University of Parma, Parco Area delle Scienze, 157/A, Parma, Italy*
[c] *Department of Geosciences, Freie Universität Berlin, Berlin, Germany*

A B S T R A C T

The Sicily Channel is characterized by the presence of prominent WNW-oriented grabens (Pantelleria, Malta, Linosa Graben) which would point out a main extensional phase within this part of the northern African plate. However, the analysis of both seismic and wells data shows evidence of tectonic reactivation and contractional events in a N-S oriented band crossing the Gela Thrust System and the Malta and Linosa Grabens. We present and discuss the timing of the different deformation phases and their potential geodynamic framework with regard to the regional Africa and Europe convergence. We suggest four main deformation phases affecting the Sicily Channel in Neogene time: 1) a contractional phase, related to the thrusting of the Sicily Fold-and-Thrust Belt in the Upper Miocene, related to the evolution of the regional Western Mediterranean Subduction Zone, 2) an extensional phase with the opening of the main grabens in Lower Pliocene, related to the fast rollback of the Calabrian Slab to the East-Southeast of the Sicily Channel, 3) a Plio-Pleistocene contractional phase with inversion structures within the grabens and onset of transpressive deformation along the Capo Granitola-Sciacca Fault Zone (CGSFZ) and Scicli Ragusa Fault System (SRFS), related to the advance of the Gela Thrust System, and 4) a presently active, mild contractional phase affecting the area between the CGFFZ and SRFS, in particular the Malta and Linosa Graben, which might be related to a regional plate reorganization and potential subduction polarity switch north of Sicily.

1. Introduction

The "Sicily Channel Rift Zone" (SCRZ; Finetti, 1984) is considered a great example of passive rifting that occurred during the Lower Pliocene (Reuther and Eisbacher, 1985; Boccaletti et al., 1987; Cello, 1987; Civile et al., 2010) in the Mediterranean area. It is widely known that crustal thinning and the formation of the WNW-oriented graben of Pantelleria, Linosa and Malta, which form the SCRZ, here coexist with the Sicilian Fold and Thrust Belt (Gela Thrust System), an expression of the Africa-Europe convergence (Fig. 1). The presence of both extensional and contractional structures has been demonstrated and analyzed by several authors (e.g., Finetti, 1984; Civile et al., 2010; Civile et al., 2021; Sulli et al., 2021). The Sicily Channel is therefore a key area to study coexisting, diverse tectonic and geodynamic processes.

The convergence of the European and African plates was associated with southward roll-back of the African slab in the Western-Central

Mediterranean, causing the opening of the Tyrrhenian back-arc basin in the overlaying plate (Faccenna et al., 2001a, 2001b; Corti et al., 2006) contemporaneously with the formation of several extensional structures in the Sicily Channel (Argnani, 1990) in Mio-Pliocene times. A passive rifting process is widely accepted to explain the extensional structures and the local crustal thinning of the Sicily Channel but in the frame of not complete coverage of seismic crustal data (Finetti, 1984; Civile et al., 2010; Civile et al., 2021). Many authors suggest that the extension was induced by two dextral strike-slip faults, which led to the formation of pull-apart basins (Jongsma et al., 1985; Reuther and Eisbacher, 1985; Boccaletti et al., 1987; Catalano et al., 2009). Instead, Argnani (1990) and Argnani (2009) suggested that the rifting process was triggered by mantle convection developed during the roll-back of the African slab beneath the Tyrrhenian Basin. In particular, they considered the crustal stretching of the SCRZ to be caused by slab-pull forces, the consequent trench retreat and roll-back, and, ultimately, the break-off of the slab.

Furthermore, among the most recent hypothesis, Arab et al. (2020) linked the extension of the Sicily Channel to the presence of a subduction transform edge propagation (STEP) fault or eastward slab tearing within the African continental lithosphere (Tunisian-Atlas Tear) segmenting the northward subducting African slab and facilitating the slab-retreat (Govers and Wortel, 2005; Rosenbaum et al., 2008). Other authors, such as Corti et al. (2006), consider however the accretion of the Sicilian Maghrebian chain and rifting in the Sicily Channel as two independent tectonic processes acting simultaneously.

In addition to the various hypotheses proposed to explain the extension in the Sicily Channel, local variations of the African continental crust thickness need to be considered. The latter shows a medium value of 25–30 km in the Mediterranean area (Finetti, 1984; Finetti and Del Ben, 2005; Micallef et al., 2019) and it decreases to 12–15 km at the current Gela Front, which is more advanced than the surrounding areas due to a less thick crust (Catalano et al., 2000; Civile et al., 2008). Seismic and gravimetric data also shows that the crust is less than 20 km (with local Moho's rising) in the Pantelleria, Linosa, and Malta basins (Scarascia et al., 1994; Finetti and Del Ben, 2005; Agius et al., 2022). Much uncertainty in this area relates to the timing and the causes of positive inversions in the Sicily Channel area (Civile et al., 2008). In the onshore sector, the presence of an active convergence between Europe and Africa has led to the development of north-verging thrusting in the northern Sicily continental margin (Sulli et al., 2021). Instead, in the
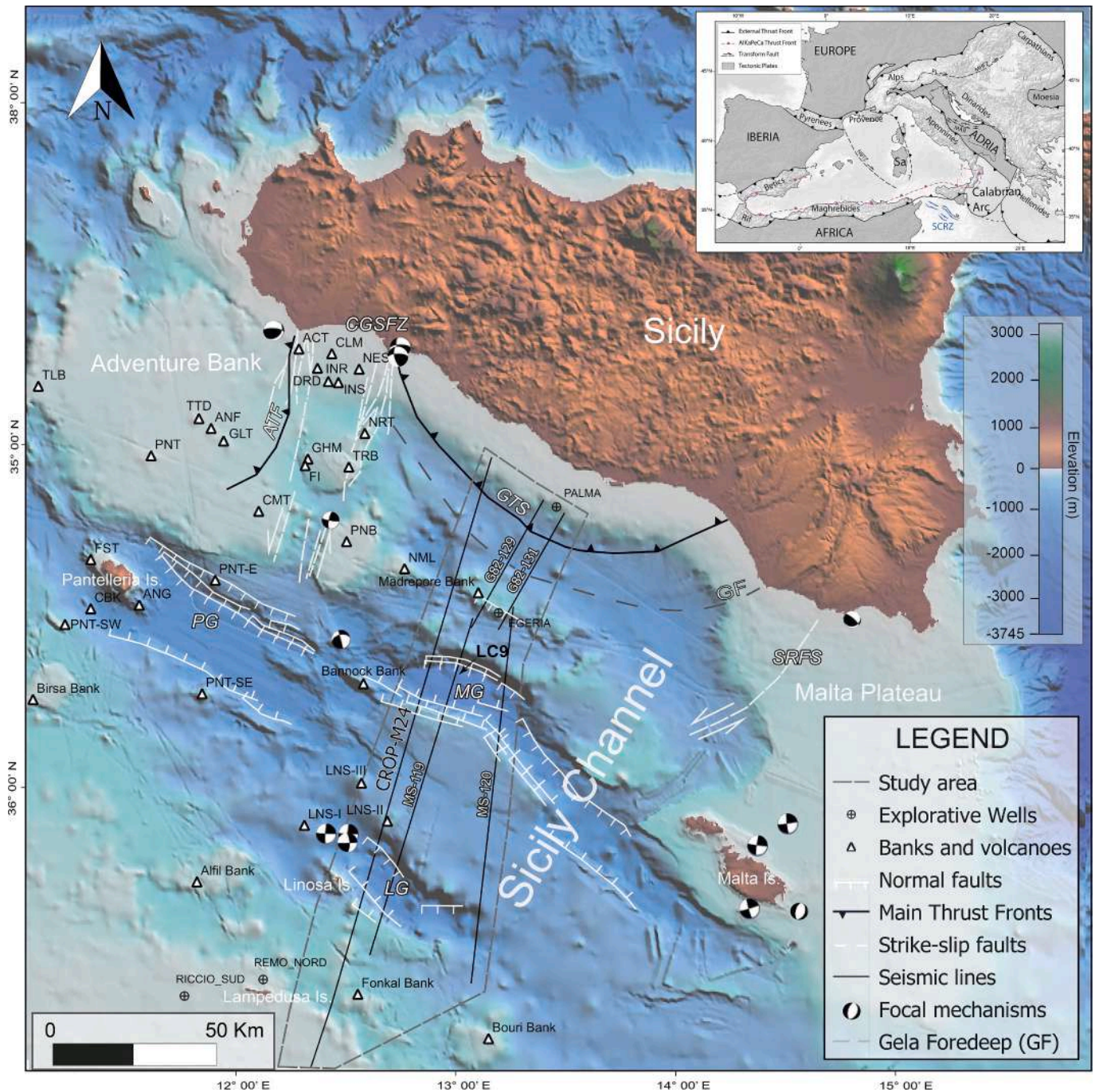

Fig. 1. Bathymetric data from GEBCO (https://www.gebco.net/) showing the main morphological and structural elements. 1: Adventure Bank; 2: Graham Bank, 3: Pantelleria Bank, 4: Talbot Bank, 5: Birsa Bank, 6.: Alfil Bank, 7: Fonkal bank, 8: Bouri bank, 9: Malta Plateau, 10: Madrepore Bank, 11: Falda di Gela, 12: Gela Basin, 13: Malta Graben, 14: Linosa Graben, 15: Pantelleria Graben, 16: Nameless Bank, 17: Linosa Plateau.

offshore sector, Cavallaro et al. (2017) linked the evidence of a positive tectonic reactivation in this area to the onset of a complex poly-phasic advancing of the Gela Thrust System whose deformation extends to the north-central sector of the Sicily Channel. But it has not been detected how far in the Sicilian offshore this compression extends. This work aims to delineate the distribution and the chronology of the compressive and extensional geological events along a N-S-oriented band crossing the central Sicily Channel, from the Gela Thrust System to the Linosa Graben (Fig. 1) in order to outline the main driving forces and improve the knowledge about the geodynamic framework that shaped the study area.

2. Geological setting

2.1. Tectonic setting

The Sicily Channel area (Fig. 1) is located in the foreland area of the Sicilian Fold and Thrust Belt which formed due to the convergence between the European and African Plates. For a better understanding of the geodynamic setting of the Sicily Channel, it is necessary to consider the tectonic evolution of the Central Mediterranean area. A phase of divergence between Europe and Africa led to the opening of the Alpine Tethys Ocean in the Mesozoic (Catalano and D'Argenio, 1982; Jongsma et al., 1985; Stampfli, 2005; Handy et al., 2010; Van Hinsbergen et al., 2020; Le Breton et al., 2021). This event was followed by the closure of the Alpine Tethys, starting in Cretaceous time, which caused the dissection of the preexisting domains (Catalano and D'Argenio, 1982; Casero et al., 1984; Antonelli et al., 1988; Catalano et al., 2000; Basilone, 2009). A second extensional event characterized by a diffuse extension in the Sirte and Tripolitania Basin of Tunisia occurred in the Lower Cretaceous and was related to a major rifting event in Central Africa (Stampfli et al., 2001). In the Upper Cretaceous-Middle Eocene, the Central Mediterranean was dominated by a NW-SE-oriented compressive stress field (Antonelli et al., 1988; Torelli et al., 1995) coeval to a change in African Plate motion that started to move towards the North, due to the opening of the South Atlantic (Stampfli and Borel, 2002, Stampfli, 2005; Handy et al., 2010; Van Hinsbergen et al., 2020; Le Breton et al., 2021). During the Upper Oligocene-Lower Miocene, the rollback of the Western Mediterranean subduction resulted in upper-plate extension, opening of the Liguro-Provencal Basin and counter-clockwise rotation of the Sardinia-Corsica, coevally to the accretion of the Sicilian Fold and Thrust Belt (Speranza et al., 2018). The evolution of the Mediterranean area was abruptly marked in the Late Messinian by the isolation of the Mediterranean basin from the Atlantic; this event was called the "Messinian Salinity Crisis" (Hsü et al., 1973; Butler et al., 1995; Andreetto et al., 2021). The sedimentation of considerable width and locally very thick, up to 3 km, of evaporative deposits, allows us to have a seismic marker of the Messinian age in the entire Mediterranean basin (Lofi et al., 2011; Roveri et al., 2014; Haq et al., 2020). During the Messinian Salinity Crisis, most of the banks/seamounts of the Sicily Channel emerged and underwent a diffuse erosion (Civile et al., 2015). Later, during the Lower Pliocene, an extensional event led to the formation of the Malta, Linosa, and Pantelleria WNW-ESE-oriented depressions (Grasso and Torelli, 1999; Carminati and Doglioni, 2005; Civile et al., 2010; Ghielmi et al., 2012; Civile et al., 2021) (Fig. 1). The closeness of the Sicilian Fold and Thrust Belt is considered to be the cause of the local superposition of contractional structures on the pre-existing extensional system in the north-central sector of the Sicily Channel (Cavallaro et al., 2017). However, even in inland Sicily and inside the fold-and-thrust belt, north-verging thrusts and double-verging thrust systems have been recently evidenced and documented as back-thrusting (Sulli et al., 2021).

2.2. Morphostructural setting

Within the Sicily Channel, several morphostructural highs and basins can be observed (Fig. 1). Offshore Sicily, the first morphological element is the Adventure Bank to the west (Fig. 1), which is a wide shallow platform occupied by the outermost front of the Sicilian Fold and Thrust Belt, called the Adventure Thrust Front (ATF in Fig. 1; Argnani, 1990) and its foredeep, the Adventure Foredeep (AF in Fig. 1; Antonelli et al., 1988; Argnani, 1990). The AF is affected by a regional tectonic structure named the Capo Granitola-Sciacca Fault Zone (CGSFZ in Fig. 1). The CGSFZ is a wide structure developed in the Lower Pliocene that shows a left-lateral kinematic movement active in the Quaternary period (Civile et al., 2018). To the East, the Gela Foredeep (GF in Fig. 1) is a Plio-Quaternary foredeep developed in front of the south-verging Plio-Pleistocene Gela Thrust System (GTS; Argnani, 1990; Butler et al., 1992; Catalano et al., 2013; Lickorish et al., 1999). East of the GTS, the Malta Plateau forms another shallow shelf zone (Todaro et al., 2021), which hosts the Scicli Ragusa Fault System (SRFS in Fig. 1), a wide structure showing also a left-lateral movement in the last 0.85 Ma (Catalano et al., 2008). In the central part of the Sicily Channel, the Pantelleria (PG), Malta (MG), and Linosa (LG) grabens form distinct WNW-ESE-oriented narrow (c. 10–25 km wide) and elongated (c. 50–120 km long) morphostructural features. Spread throughout the area, extending to the limit to the Tunisian continental shelf, several small seamounts and seamount-like structures are observed (Fig. 1; Aissi et al., 2015).

2.3. Magmatism

Throughout the Sicily Channel, magmatic manifestations are widespread (Fig. 1) and have long been investigated through seismic reflection profiles and bathymetric data. The oldest magmatic activity is registered by Beccaluva et al. (1981) in the Nameless Bank (NML in Fig. 1) in the late Miocene (9.5 ± 0.4 Ma). The main volcanic manifestations of the Sicily Channel that occurred in the Plio-Pleistocene during the Sicily Channel's extension are registered in the Graham and Terrible Bank (GHM and TRB in Fig. 1). Volcanism is mainly concentrated in Pantelleria and Linosa islands (Lodolo et al., 2012). In fact, the Pantelleria island consists of a volcanic building that develops partly above sea level. Some volcanic seamounts (e.g. Angelina, ANG in Fig. 1) extend around the Pantelleria Graben axis suggesting a volcano-tectonic origin (Civile et al., 2010; Lodolo et al., 2012). The Linosa island, which emerged in the Quaternary age, shows volcanic activity dated from 1.06 to 0.5 Ma (Lanzafame et al., 1994) with an alkaline composition on the outcropping rocks (Romagnoli et al., 2020). and a main NW-SE trend. Near Linosa several volcanic centers occur, e.g. Linosa I, II, III (LNS I, II, III in Fig. 1; Lodolo et al., 2012). Indeed, recent bathymetric data reveal that the emergent part of Linosa represents only about 3.6% percentage of the entire volcanic complex (about 165 km^2). This shows how much uncertainty there still is about the submarine extension of the volcanic product of the area (Tonielli et al., 2019). Among the most recent magmatic manifestations, six volcanic edifices were formed following a tectonic event that occurred near the CGSFZ (Fig. 1). Their magmatic activity is dated pre-Last Glacial Maximum (LGM, ca. 20 ka B.P.), except for Actea volcano (ACT, Fig. 1), which shows post-LGM volcanism (Lodolo et al., 2019). Other important and recent eruptions are the ones that occurred in 1831 in the Graham Bank of Ferdinandea Island (FI in Fig. 1) and in 1981 near Pantelleria Island, approximately 5 km NW of the island (Washington, 1909).

2.4. Seismicity

The Sicily Channel's seismicity has been generally related to the several tectonic processes coexisting in the area, in particular to the Europe-Africa convergence. Seismic activity in the Sicily Channel area is considered moderate, despite the complex setting. Different focal mechanisms available by the INGV database (ISIDe Working Group, 2007; https://emidius.mi.ingv.it/CPTI15-DBMI15/query_place/ highlight a widespread strike-slip type of movement (Palano et al., 2012; Fig. 1). Seismological studies show the presence of two main seismic

fault zones in Sicily, respectively to the east and the west of the Gela Thrust System, extending offshore into the Sicily Channel. The first to the west has a NNE-SSW direction, from Sciacca to Linosa island, and corresponds to the CGSFZ (Fig. 1; Civile et al., 2018; Ferranti et al., 2019; Civile et al., 2021). In this sector, it is also documented the presence of several earthquakes with a left-lateral strike-slip deformation, volcanic manifestation and high heat flow (Palano et al., 2020). Geochemical and seismic evidence shows that this system develops down to the upper mantle (70 km depth), involving a lithospheric discontinuity that could not be related to a rifting process (Caracausi et al., 2005; Calò and Parisi, 2014). The other fault zone to the east of the Gela Thrust System, is the Scicli Ragusa Fault System (SRFS), which develops from the southeastern sector of Sicily, from Ragusa to the Sicily Channel offshore, with an undetermined length (Fig. 1). A left-lateral strike-slip activity has been detected in the whole fault zone (Catalano et al., 2008), and is related to the development of both restraining and releasing bends geometries between the distinct en-echelon segments (Grasso and Reuther, 1988). Moreover, in the Maltese archipelago focal mechanisms of recent earthquakes show evidence of right-lateral strike-slip faults (Fig. 1) (Micallef et al., 2019).

2.5. Geodetic data

The convergence between Africa and Europe, based on GPS measurements, has an average rate of 4–5 mm/yr (Sulli et al., 2021). The available data of the different GPS stations of Sicily (Fig. 2) show a higher velocity in the SE, at the NOTO station, with an average value of 4.7 mm/yr and a NNW direction. In the NW sector of Sicily, the MILO station, shows an average velocity of 3.6 mm/yr, with a NNW direction (Hollenstein et al., 2003; D'Agostino and Selvaggi, 2004; Serpelloni et al., 2005, Devoti et al., 2011; Palano et al., 2012, Sulli et al., 2021). GPS data acquired in the Sicily Channel indicate that Pantelleria (PZIN) moves towards SSE with a 2.95 mm/yr medium rate and Lampedusa (LAMP) moves towards SSE with a 1 mm/yr velocity (Fig. 2). Malta (MALT) moves towards NNW (Fig. 2) with an average rate of 1.5 mm/yr (Palano et al., 2012). These movements imply an ongoing convergence between the two islands with a NW-SE convergence and a NE-SW stretching direction between Lampedusa and Malta (Meccariello et al., 2017).

2.6. Gravimetric anomalies

The highest positive anomaly in the Sicily Channel was detected near the Pantelleria depression, with a value of +70 mgal (Fig. 2) (Sandwell et al., 2013). Other highest values, +60, and + 65 mgal (Fig. 2), are recorded in the areas of Nameless Bank, Graham Bank and Adventure Bank (Sandwell et al., 2013). Those anomalies, also linked to magnetic anomalies, have been associated to the presence of buried magmatic bodies (Lodolo et al., 2012) which has been linked to a Moho's rising at relatively shallow depths below them, up to 17–18 km (Finetti and Del Ben, 2005; Civile et al., 2008). Negative values of Bouguer's anomaly, −40 mgal, are recorded in correspondence to the Gela Thrust System (Sandwell et al., 2013) (Fig. 2). This has been related to a Moho deepening up to 36 km depth beneath the Gela Thurst System (Finetti and Del
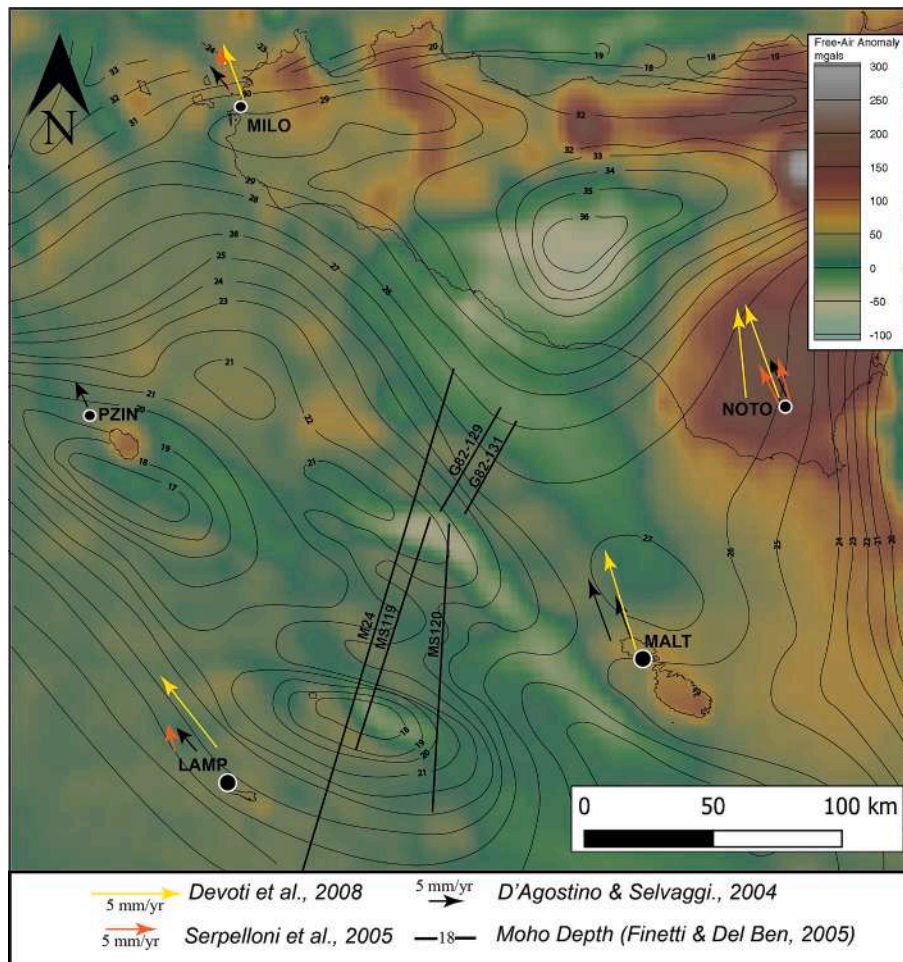

Fig. 2. Map showing gravimetry model from Sandwell et al. (2013), Moho contour lines, and available data of the different GPS stations of the study area GPS velocity vectors with respect to Eurasia according to different authors; the location of the analyzed seismic reflection profiles is also reported.

Table 1

Recording parameters for MS119, MS120, G82–131 01–04, G82–129, M24 lines.

Lines	MS 119,120
Recording date	Aug.-Sep. 1980
Sample rate	4 ms
Tape format	SEG-B/9 TRACKS
Filters	Low cut 8 Hz
	High cut 62 Hz
	Notch IN
	Alias 62 Hz
Gain	IFP
	Contant 24 dB
Streamer	Seco-multidyne
Gable length	2350 M
Number of traces	48
Group interval	50 m
Hydrophone group	46
Group length	100 m
Deep of streamer	20 m
Energy source	Flexotir
Filter	8/12–62 Hz
Coverage	1200 x

Line	M24
Recording date	November 1993
Sample rate	4 ms
Shot interval	50 m
Recording length	1700 ms
Filters	High cut 77 Hz
Group interval	25 m
Group	120
Depth	8 m
Energy source	Air Gun
Coverage	30-fold

Lines	G82–131 01–04, G82–129
Recording date	May 1982
Sample rate	2 ms
Tape format	SEG-B/9 TRACKS
Filters	Low cut 8 Hz
	High cut 128 Hz
	Notch IN
Group interval	25 m
Group	96
Depth	6.5 m
Energy source	Air Gun
SP interval	8/12–62 Hz
Coverage	1200 x

Ben, 2005).

3. Materials and methods

3.1. Materials

To achieve the goals of this study, data collected by the ViDEPI (Visibility of petroleum exploration data in Italy) Project have been analyzed (https://www.videpi.com/videpi/videpi.asp) where well-logs and reflection seismic data are available. More specifically, we used seismic data from the CROP Project (Deep Seismic Exploration of the Central Mediterranean and Italy; http://www.crop.cnr.it/) and from reconnaissance seismic campaigns of Italian offshore areas (Zone G) acquired by AGIP, on behalf of the Italian State. The CROP marine dataset was performed from 1988 to 1995 by the RV OGS-Explora with an Airgun array and a 4500 m long and 180-channel streamer (Finetti and Del Ben, 2005). The profiles of the G dataset were acquired with the Airgun with a sampling interval of 4 ms (250 Hz), a 6–7 s acquisition

Table 2

Processing parameters for MS119, MS120, G82–131 01–04, G82–129, M24 lines.

Lines	MS120, MS122
Processed length	10–12 s
Sample rate	4 ms
Pre-processed	CDP GATHER
T.V. deconvolution	3 zones
Velocity A.N. location	N.M.O. corr. and 12-fold stack
Display	Wiggle V.A. 2.5 in./s. 25 traces

Lines	G82–131 01–04, G82–129
Trace merging	5/4
Resample	4 ms
Air gun delay	51 ms
Length	200 ms
Stack	4800
Time variant filters	12/65 Hz
	4/98 Hz
Traces	80/km

Line	M24
Resample	8 ms
Channel reduction	To 90
F-K Filter	2–12 ms
Analysis interval	15 km

window and 4800% coverage and 1:25000 scale (ViDEPI). Data derived also from the Mediterranean Sea project (MS) that covered extensive areas of the Mediterranean Sea, performed by the Osservatorio Geofisico Sperimentale (OGS) of Trieste from 1969 to 1982 were also analyzed (Finetti and Morelli, 1973a, 1973b). In order to improve the quality of some seismic reflection profiles, we realized a conversion from ViDEPI PDF seismic profile to SEG-Y format by using Tif2segy tool. Further, migration has been applied through SeisUnix software, to reduce diffraction hyperbolae zones. The seismic reflection profiles presented in this work (location on Fig. 1) and their recording and processing parameters are reported and Table 1 and Table 2. CROP M24, a high penetration seismic reflection profile has been analyzed to constrain the crustal setting of the area. The wells Egeria and Palma were used to constrain the stratigraphy of the northern part of the study area. Otherwise, Riccio Sud and Remo Nord wells were analyzed to constrain the stratigraphy of the southern part of the study area. The LC9 sampling (Fig. 1), by Reeder et al. (2002), defines the characteristics of the shallow filling of the Malta Graben, up to 26 m b.s.l.. In detail, it shows the presence of volcanic tephra at about 9 m deep, and the presence of faults from 15 to 18 m deep.

3.2. Methods

3.2.1. Interpretation of seismic reflection profiles: Seismo-stratigraphic and structural analysis

An interpretation of the seismic reflection profiles has been carried out using dedicated graphic design programs. Different seismic facies have been identified by reflection attributes such as amplitude, frequency, and lateral continuity as well as their lateral terminations (onlap, downlap, toplap) and reflection patterns following the seismic reflection profile interpretation technique (Vail, 1987; Hart, 2010). The most continuous and geologically meaningful, as derived after well-log calibration, reflectors have been mapped and the units have been correlated with the Egeria, Palma, Riccio Sud, and Remo Nord wells. The seismic stratigraphic analysis has been based on the identification of different characteristics of the reflections; namely amplitude, frequency, continuity, and configuration patterns (parallel, divergent, etc.) according to the procedure described in Mitchum et al. (1977). Different

Table 3

Seismic facies and topping horizons definition and description of the main seismic lines based on Vail (1987) method.

Seismic Facies/ Topping horizon	Description	Seismic signal
S11/Seabed	Reflectors with high amplitude, low frequency, and parallel (locally chaotic) geometry, with onlap termination on S10 facies.	
S10/L	Reflectors with medium amplitude, medium/low frequency, and parallel geometry, with onlap termination on S7 facies. In the Linosa Plateau sector, the reflectors show high amplitude, low frequency, and an oblique parallel reflection configuration with a downlap termination on the S9 facies.	
S9/I	Reflectors with medium amplitude, low frequency, and parallel geometry, with onlap termination on S7 facies.	
S8/H	Chaotic reflectors with a transparent signal upwards. This facies shows a convergent geometry in the Malta Graben, Linosa Graben.	
S7/G	Reflectors with high amplitude and low frequency, with a locally chaotic configuration interrupted by semi-transparent zones.	
S6/F	Facies with high frequency, low amplitude and a parallel configuration. Locally interrupted by diffraction hyperbola zones. Locally it shows an erosive truncation.	
S5/E	Reflectors with high-medium amplitude, high continuity, high frequency and a parallel configuration. Frequently interrupted by diffraction hyperbola zones and dissected by several normal faults.	
S4/D	Reflectors with high amplitude, high continuity, medium frequency, and a subparallel configuration. Locally with chaotic configuration. Frequently interrupted by diffraction hyperbola and dissected by normal faults.	
S3/C	Layered signal, with high-medium amplitude, medium continuity, low frequency, and a subparallel configuration, frequently interrupted by diffraction hyperbola zones.	
S2/B	Poorly layered signal, with medium amplitude, low continuity, low frequency, and a subparallel configuration, locally interrupted by diffraction hyperbola zones.	
S1/A	Discontinuous signal, with high amplitude, low frequency, and a chaotic configuration; topped by double high-amplitude reflections, locally interrupted by diffraction hyperbola arranged in a mound-shaped body.	

seismic facies, bounded by 11 key reflections named A-L and including seafloor reflection, have been identified in the analyzed seismic profiles. These seismic facies are reported in Table 3. The key reflectors are used as markers to identify structural features deforming the Sicily Channel.

3.2.2. Depth-to-time conversion of selected well-logs

In order to constrain the seismo-stratigraphic interpretation, the Egeria and Palma wells were projected onto the closest seismic reflection profiles (G82–131, G82–129, M24; Fig. 1). The wells could be projected in time because of the sonic log velocities reported in the final log. In Tables 1–4 of Suppl. Mat., the well-logs data of thickness, lithology, and depth for each lithological unit and the interval velocity obtained from the average microsec./ft. in the sonic log are reported. Instead, Riccio Sud and Remo Nord, with no sonic log, were depth-converted using standard velocities for each lithology (Christensen and Mooney, 1995) (Suppl. Mat., Table 5) and then projected onto the CROP M24 seismic lines.

3.2.3. Seismic reflection profiles calibration and well-tie

The reflectors with the highest contrasts in acoustic impedance were compared to the major lithological contacts/changes reported in the well-logs. This comparison allowed us to verify the corresponding position of the main stratigraphic contacts in the time domain. This step was needed to calibrate the seismo-stratigraphic units and the main horizons identified in the seismic lines. The well-logs calibration was integrated with literature data and the lateral variability of the stratigraphic units was evidenced by stratigraphic correlations among the four wells available after establishing a comparative table of stratigraphic successions known on the Tunisian margin and in inland Sicily (Table 6 in Suppl. Mat.). The seismic calibration was mainly based on the stratigraphic logs of the Palma, Egeria, Riccio Sud, and Remo Nord's wells (Fig. 3). Once the wells were located on the closest seismic reflection profiles, each horizon was identified and traced in the profiles and over the maximum extent of the survey (Fig. 4).

4. Results

The recognized seismic facies (Table 3), well-log stratigraphic correlation (Fig. 3), well-log tied to seismic reflection profiles, seismo-stratigraphic and structural interpretation (Figs. 4–11) are presented below. The shallow portions (down to ~3 s) were calibrated with the well-log data, while the interpretations of the deep portions are mainly based on the M24 seismic line and the literature data (Finetti and Del Ben, 2005).

4.1. Seismic facies, seismo-stratigraphic units, and well-tie

The lowermost seismic facies (S1) detected in the CROP M24 seismic line, is marked at the top by double high-amplitude reflections (A) (Table 3). Horizon A shows low continuity and high reflectivity, it is located at an average depth of 11.4 s/TWT (Table 3, Figs. 4, 5). The seismic facies S1 shows widespread hyperbolae zones with a mound-shaped body arrangement that is concentrated in correspondence of the Linosa and Malta Grabens, interrupting the lateral continuity of the signal (Table 3, Figs. 4, 5). There the Horizon A also shows a mild rising to 10 s/TWT and it deepens towards the Gela Thrust System down to 12.8 s/TWT (Fig. 4). The overlying seismic facies (S2) appears poorly layered and topped by the Horizon B, which shows high amplitude and discontinuous reflector (Table 3, Figs. 4, 5). It appears at an average depth of 6 s/TWT and deepens to 11 s/TWT towards the Gela Thrust System (Fig. 4). Like the previous seismic facies, it is locally interrupted by a mound-shaped body rich in hyperbola, attributed to fluid rising based on similar signals highlighted in literature data (ex. Tonga Trench, Bally, 1983). Reflector A has been identified as the Moho surface while the Horizon B (Table 3, Figs. 4, 5) has been attributed to the top of the Upper Crust; as deep drills and logs are missing, this attribution was

based on literature data (Finetti and Del Ben, 2005; Scarascia et al., 1994) and seismic attributes analysis. The following seismic facies have been calibrated with well-log data (Suppl. Mat. Table 1–4) and projected onto the seismic lines. The S3 facies is bounded at the top by the Horizon C, which corresponds to the top of the Jurassic formations (Buccheri Fm., Nara Fm., Sidi Kralif Fm.) (Fig. 3 and Table 6 Suppl. Mat.). Horizon C appears to be affected by several normal faults and is locally interrupted by diffraction hyperbola mounds, attributed to magmatic intrusions based on the seismic signal and the Egeria's well-log evidence (Fig. 3).

The facies S4 is topped by Horizon D which is a high amplitude reflector (Table 3) dissected by several normal faults. The S4 facies corresponds to the Early Cretaceous Formations (Sidi Kralif Fm., Hybla Fm., Gebel Nehal Fm., Bou Hedna Fm., Sidi Aich Fm., Serd J Fm., Hammeima Fm., Fadhene Fm.) (Suppl. Mat.) that appears locally interrupted by diffraction hyperbola that has been still associated with magmatic intrusions, although no evidence of igneous rock has been detected in the analyzed well-logs (Figs. 3, 4, 5).

The facies S5, topped by Horizon E (Table 3), appear highly affected by faulting. It locally shows the presence of diffraction hyperbola attributed to magmatic intrusions, based on the Remo Nord well-log. This facies S5 has been interpreted as the Paleocene-Eocene units (Amerillo Fm.) (Fig. 3 and Suppl. Mat. Table 6). The facies S6 is topped by the Horizon F and corresponds to the Oligocene-Lower Miocene formation (Ragusa Fm.) (Figs. 4, 7). Horizon F is a discontinuous reflector that marks an erosional truncation, it is highly interrupted by normal faults and diffraction hyperbola. Facies S7 is topped by the Horizon G (Table 3, Figs. 4–10) corresponding to the top of the Messinian evaporites which, in the whole Mediterranean area, identifies a marker locally associated to erosional phases (Lofi et al., 2011). Horizon G, also known as the "M-reflector", forms a typical seismic signal throughout the entire region, characterized by a high acoustic impedance contrast with high amplitude and a relatively high continuity (Lofi et al., 2011). Upward, according to biostratigraphic analysis (Di Stefano et al., 1993a), three main horizons are visible in the Plio-Pleistocene succession. They have been identified and are all related to transgressive and regressive phases (Cavallaro et al., 2017). Respectively, they are the base of Zanclean (5.33 Ma - Top of Messinian evaporites, Horizon G), the base of Gelasian (Horizon H), a 1.2 Ma unconformity (Horizon I), and a 0.8 Ma unconformity (Horizon L). The corresponding seismic facies are respectively the facies S8-S11 (Table 3), showing medium amplitude and parallel geometries, limited to each other by onlap and downlap terminations and with a progressive higher frequency upward (Table 3).

4.2. The deep crustal horizons

The M24 seismic line is a high penetration seismic profile that allows us to recognize the structures of the deep crust's layers underneath the Sicily Channel. A key element to investigate is the tracking of the Moho surface. The seismo-stratigraphic interpretation allows us to identify a maximum Moho's rise to 10 s/TWT in correspondence with the Fonkal Bank, with another possible rise in correspondence of the Linosa Graben up to 8 s/TWT (Figs. 4–6). The presence of several diffraction hyperbolae causes signal anomalies that have been linked to a rise of deep-origin fluids. In the northern part of the Sicily Channel, under the Gela Thrust System, the Moho's deepens to 11.8 s/TWT (Fig. 6 a, b). WARR (Wide Angle Reflection Refraction) velocities (Scarascia et al., 1994) allow us to carry out a depth conversion of the identified units. The calculated Moho's depth ranges from a minimum of 20 km under the Fonkal bank to a maximum of 36 km under the Gela Thrust System. The deep layers were mainly defined after the analysis of Moho's reflection characteristics. In the southernmost sector of the M24 line, the Moho rises from 11 to 10 s/TWT and is abruptly interrupted by a wide diffraction hyperbolae zone extended from 8 to 13 s/TWT underneath the Fonkal bank (Figs. 4, 5). Moho is also interrupted below the Linosa
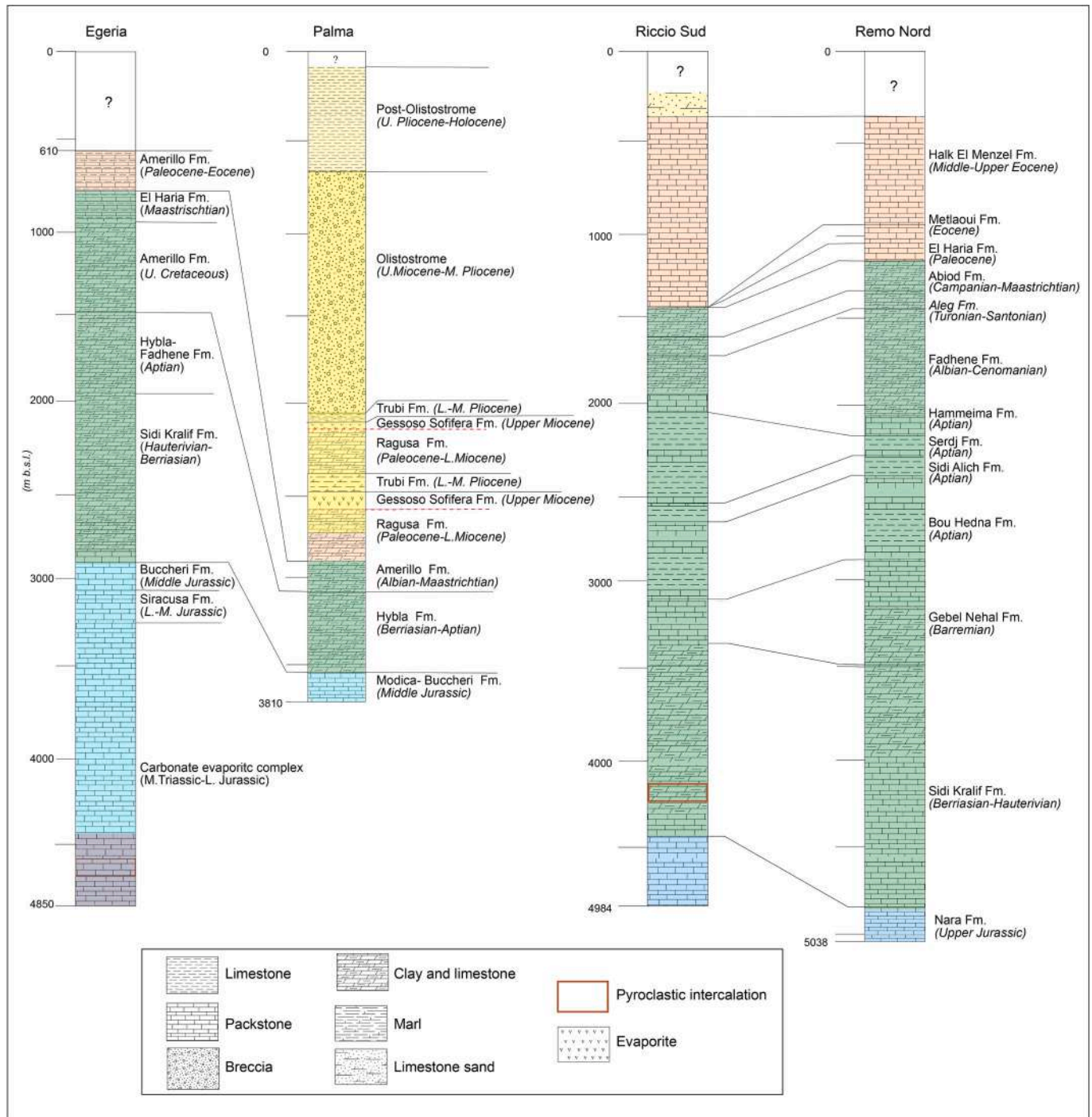
Fig. 3. Lithostratigraphic correlations of the wells respectively near the northern (Egeria and Palma, see Fig. 1) and the southern (Riccio and Remo, see Fig. 1) sector of the CROP M24 seismic line.

Graben by two wide zones rich in hyperbolae extended from 9 to 15 s /TWT (Figs. 4–6). Other Moho's interruptions are in correspondence of the Malta Graben, which extended from 8 to 14 s/TWT (Fig. 4) and under the northernmost sector where this reaches 13 s/TWT (Fig. 5 a, b). The top of the Upper Crust is located at 6 s/TWT in the southern sector of the line and deepens down to 9 s/TWT from the Linosa Plateau to the Gela Thrust System (Figs. 4-5).

4.3. The shallow structural framework

The shallow portion analysis has been divided along the main structural domains observed in the seismic data. Three main different regions have been distinguished in our study area (Fig. 1): 1) Offshore southern Sicily and the Gela Thrust System, further subdivided into the Gela Thrust System and the Madrepore bank; 2) the Central sector-Malta Graben; and 3) the Linosa-Lampedusa Sector.

4.3.1. Offshore southern Sicily and Gela Thrust system

a) Gela Thrust System

The offshore domain of southern Sicily was investigated with the
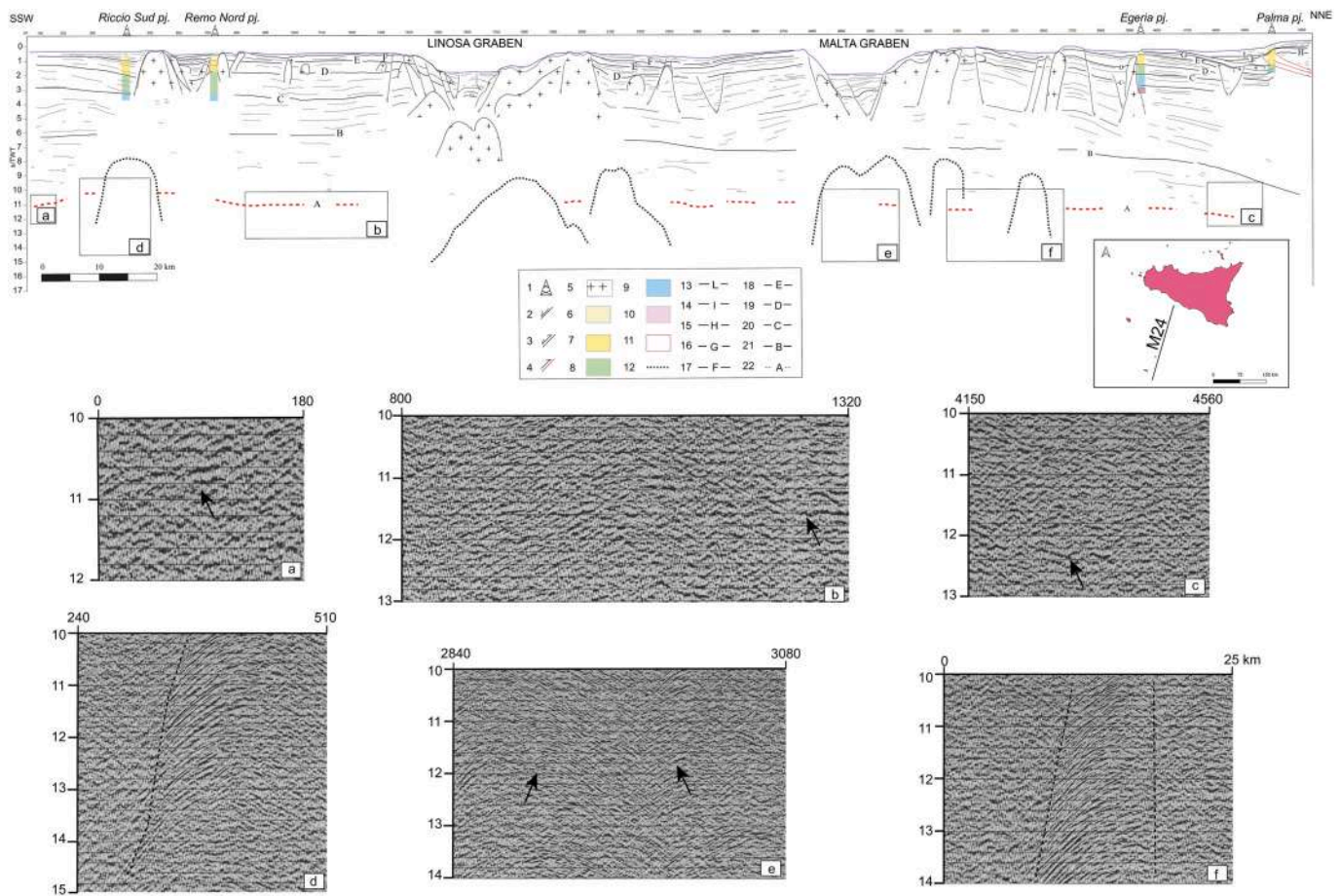
Fig. 4. Line drawing of CROP M24 seismic line with wells correlation. In the boxes below from (a) to (f) are indicated the main reflection characteristics of the deepest sectors, which show diffuse diffraction hyperbolae and high amplitude reflections. 1: well location; 2: normal fault; 3: thrust; 4: crossing seismic line; 5: volcanic intrusion; 6: Plio-Pleistocene unit; 7: Eocene-Miocene unit; 8: Cretaceous units; 9: Jurassic unit; 10: Triassic unit; 11: magmatic levels; 12: possible magmatic intrusion; 13: 0.8 Ma unconformity; 14: 1.2 Ma unconformity; 15: Base Gelasian; 16: Top Messinian Evaporites; 17: Top Oligocene unit; 18: Top Eocene unit; 19: Top Cretaceous unit; 20 top Jurassic; 21: upper crust; 22: Moho.

G82–129, G82–131, and M24 seismic profiles, where the outermost thrust of the Gela Thrust System (Gela Thrust Front) is observed (Figs. 1, 6, 7). The latter is a tectonic wedge well defined by the presence of a basal thrust that tips out towards SSW. In all the analyzed seismic lines, three key horizons, which mark the main deformation events, have been identified, respectively named H, I, and L (Figs. 6, 7). The Thrust System advancement appears to be not homogenous along strike, as testified by the presence of a more advanced thrust towards the South in the central part of the wedge also sealed by Horizon L on the G82–129 line (Fig. 7 c, d) but not on the G82–131 line (Fig. 7 a, b).

b) Madrepore bank

The southern sector of the Gela Thrust System is occupied by the associated foredeep and by the Madrepore Bank (Fig. 1). Locally reactivations of older normal faults NW-SE trending are reported in this region (Antonelli et al., 1988; Corti et al., 2006; Cavallaro et al., 2017). In the southern sector of the bank, two normal faults separate the Madrepore Bank from a depression here named Madrepore Graben (Figs. 4, 5, 8). This extends for about 9 km and shows an anticline structure, whose geometry is the result of the reactivation of pre-existing normal faults (Fig. 8 a-d), and, in line with Cavallaro et al. (2017)'s interpretation, may be affected by a positive flower structure. So far, in the Madrepore Graben two extensional phases, separated by a positive reactivation phase, have been identified on the basis of the main recognized horizons and unconformities. An old extensional phase was

identified on the basis of the Horizon G displacement by normal faults. It follows an inversion phase testified by *syn*-inversion deposits (see red square focus on Fig. 8 d) onlapping against the hinge zone of the anticlines (Fig. 8 b, d). A third event of renewed extension is observed by the presence of a mild seafloor displacement on the northernmost edge of the Madrepore Graben (Fig. 8 a-d). In the whole area, volcanic intercalations occur, detected in the Palma and Egeria well-logs and in the seismic profile, where the presence of diffraction hyperbola highlights the possible occurrence of volcanic intrusions (Figs. 3, 8).

4.3.2. Central sector-Malta Graben

In the central sector of the study area, an extensional structure called Malta Graben is observed. This is highlighted in the MS 119, MS 120, and M24 seismic lines (Figs. 4, 9 a-d). The graben's margins show chaotic/hyperbolae signals; since the evidence of volcanic tephra at 9 m b.s.l. recorded in the LC9 core by Reeder et al., 2002 (Fig. 1), and the records of similar signals along the M24 seismic line (also showing Moho rising in correspondence of these), these signals have been assumed to be magmatic intrusions with no shallow manifestation (Fig. 9 a-d), differently from Civile et al. (2021) that assumes that mass wasting deposits. Different deformation phases have been distinguished through the identification of three main unconformity surfaces (U1-U3) (Fig. 9 b, d). The Malta Graben records a younger extensional event, highlighted by the syn-rift geometry of the unit between U1 and U2 in both MS and CROP seismic lines (Fig. 9 a, b). A second event, that caused an inversion of the pre-existing structures, has been identified in the M24 and MS-119
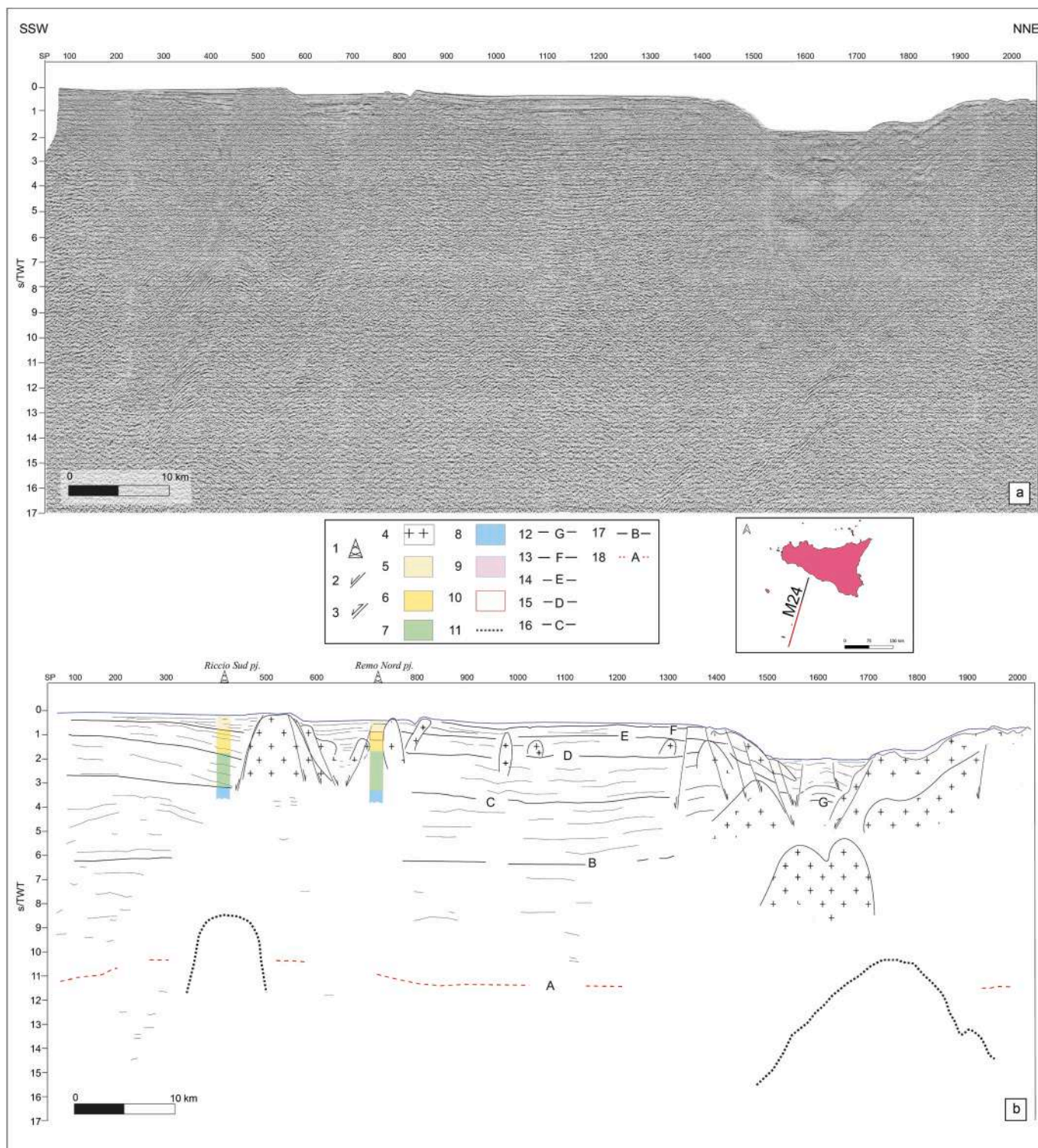
Fig. 5. (a) M24 seismic line, from the Fonkal Bank to the Linosa Graben (showed in Fig. 1) and (b) relative line drawing. 1: well location; 2: normal fault; 3: inverted fault; 4: volcanic intrusion; 5: Plio-Pleistocene unit; 6: Eocene-Miocene unit; 7: Cretaceous units; 8: Jurassic unit; 9: Triassic unit; 10: magmatic levels; 11: possible magmatic intrusion; 12: Top Messinian Evaporites; 13: Top Oligocene unit; 14: Top Eocene unit; 15: Top Cretaceous unit; 16 Top Jurassic; 17: Top upper crust; 18: Moho.

seismic lines, between the U2 and U3 unconformities. It follows a renewed extension, highlighted by the presence of normal faults intersecting the recent deposits, but only in the M24 and MS-119. However, the MS-120 shows a positive relief affecting the seabed which is uplifted of at least 500 m high (Fig. 9 a, b). The internal geometry of the Malta Graben is characterized by a roll-over anticline structure formed during

an extensional phase, its antithetic fault was inverted causing the folding of the deposits overlying the Horizon G and of the seafloor of the central Malta Graben (Fig. 9 b, d).

4.3.3. Linosa-Lampedusa Sector

Interpretation of the M24, and MS119 lines shows the presence in the
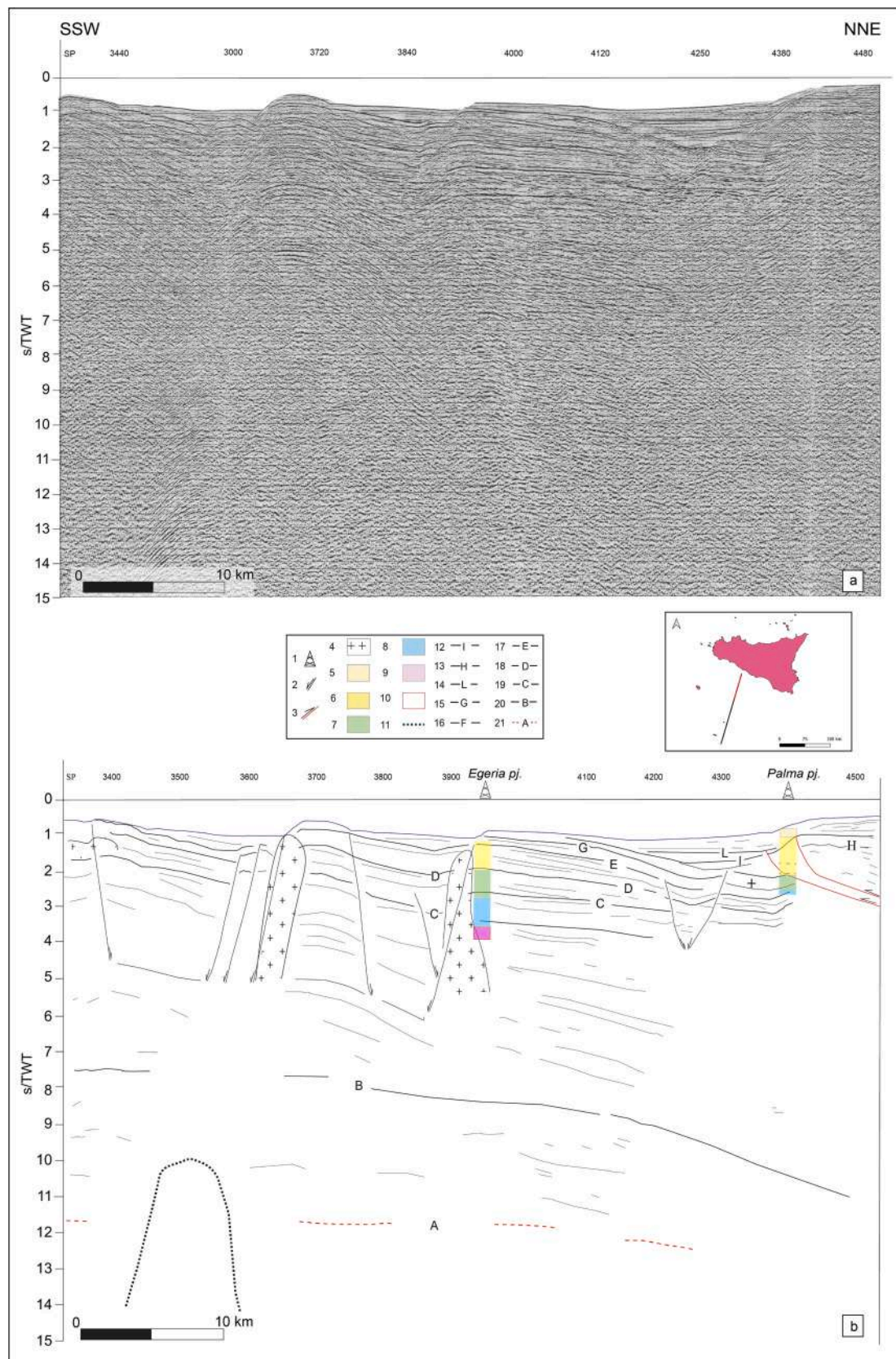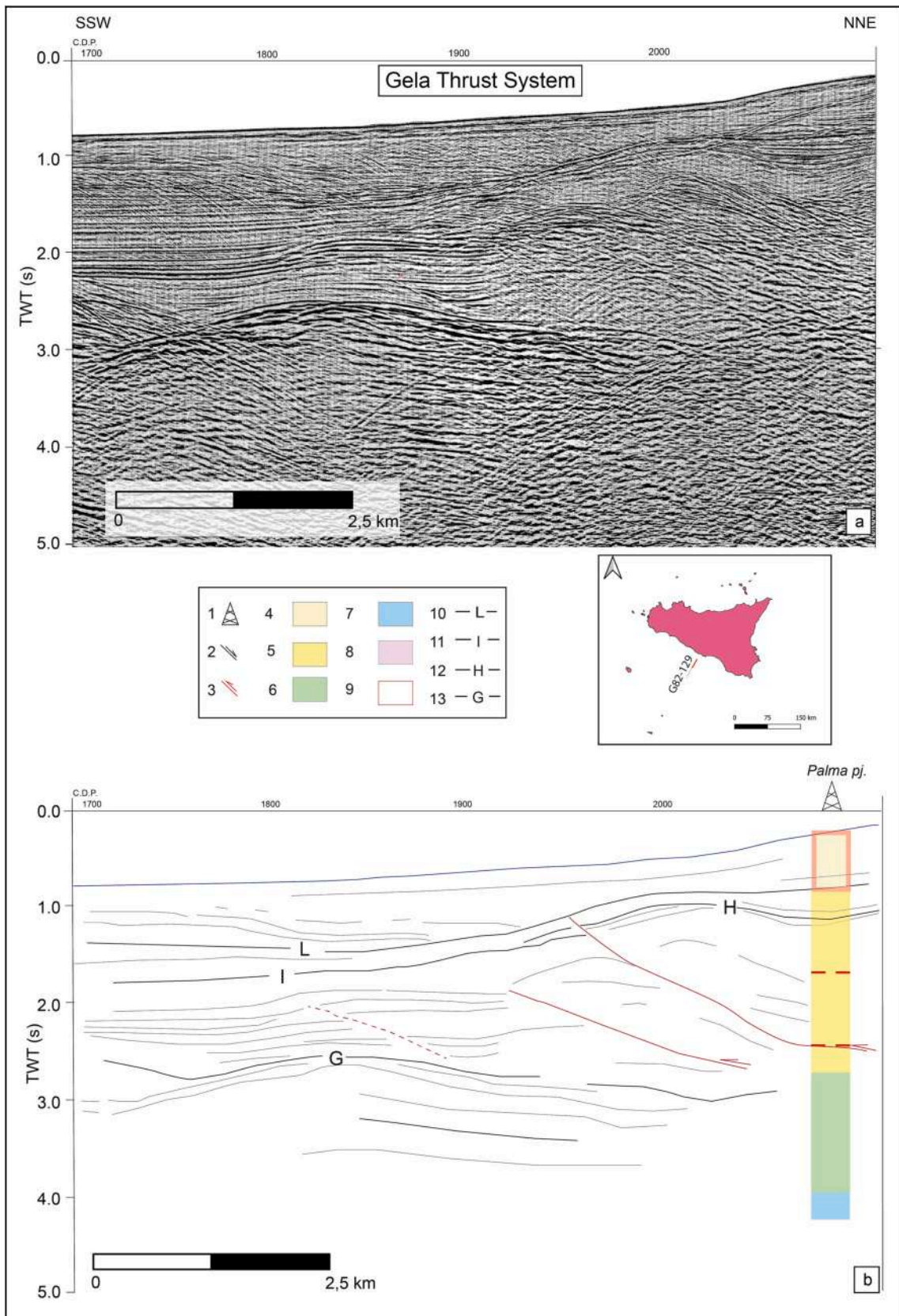
Fig. 6. (a) M24 seismic line showing the Falda di Gela sector (showed in Fig. 1) and (b) relative line drawing. 1: well location; 2: normal fault; 3: inverted fault; 4: crossing seismic line; 5: volcanic intrusion; 6: Plio-Pleistocene unit; 7: Eocene-Miocene unit; 8: Cretaceous units; 9: Jurassic unit; 10: Triassic unit; 11: magmatic levels; 12: possible magmatic intrusion; 13: 0.8 Ma unconformity; 14: 1.2 Ma unconformity; 15: Base Gelasian; 16: Top Messinian Evaporites; 17: Top Oligocene unit; 18: Top Eocene unit; 19: Top Cretaceous unit; 20 top Jurassic; 21: upper crust; 22: Moho.

Fig. 7. (a) G82 129 seismic line showing the Falda di Gela (showed in Fig. 1), and (b) the relative line drawing with Palma well log's correlation. (c) G82 131 seismic line showing Falda di Gela structure, (d) relative line drawing and correlation with Palma well log. 1: well location; 2: normal fault; 3: thrust; 4: Plio-Pleistocene unit; 5: Eocene-Miocene unit; 6: Cretaceous units; 7: Jurassic unit; 8: Triassic unit; 9: magmatic levels; 10: 0.8 Ma unconformity; 11: 1.2 Ma unconformity; 12: Base Gelasian; 13: Top Messinian Evaporites.
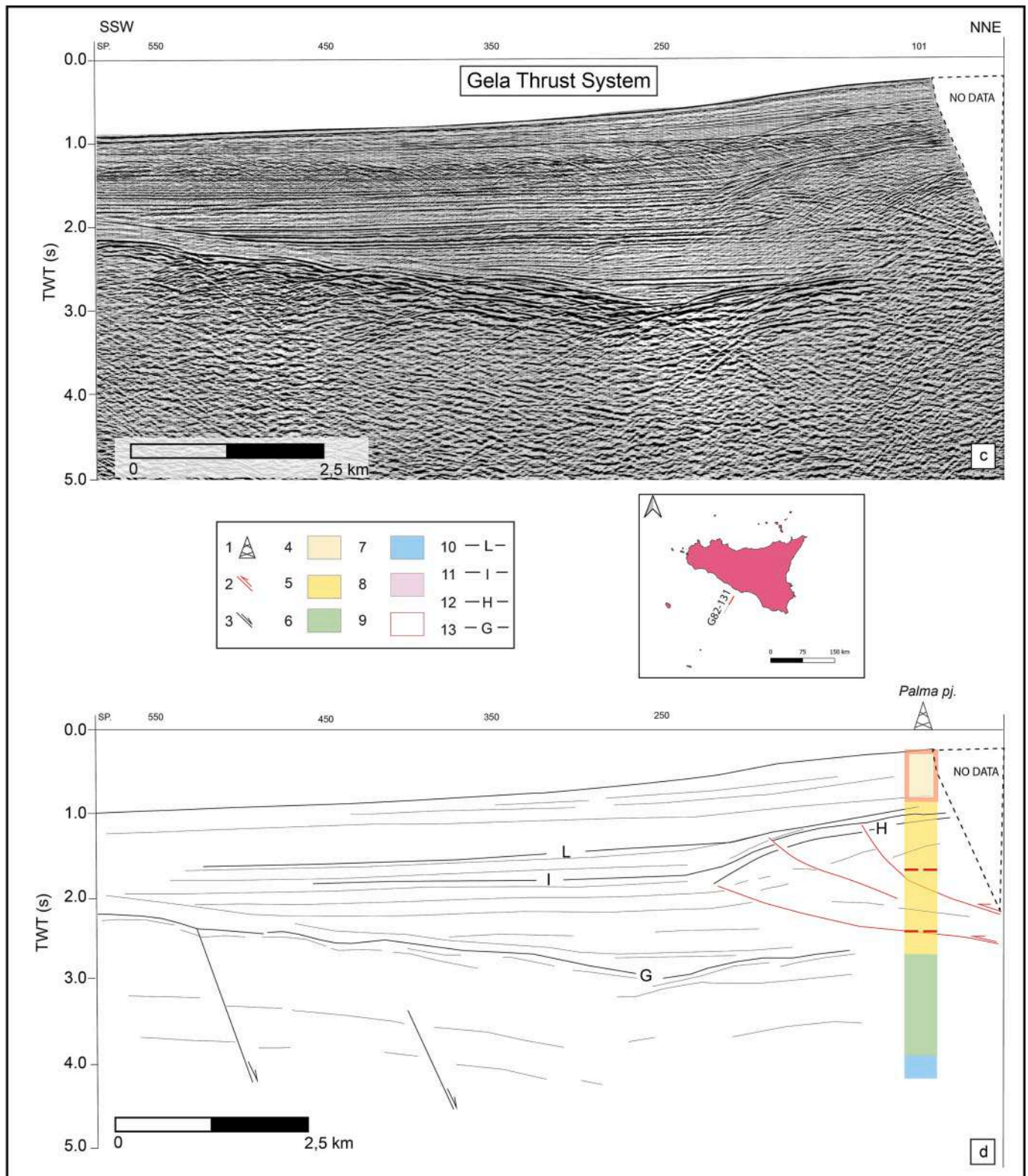
Fig. 7. (*continued*).

Lampedusa sector of a bank called Linosa Plateau and a tectonic depression named Linosa Graben (Figs. 1, 10). The Linosa Plateau is a 50 km wide bank that separates Malta and the Linosa grabens (Fig. 1). According to the seismo-stratigraphic interpretation, the G horizon appears affected by several normal faults that cause a moderate bending of the whole plateau (Fig. 10 b). These are covered by horizon I and are

overlaid by a series of prograding wedges topped by the horizon L (Fig. 10 b). The top of the wedges is 0.8 s/TWT, which is about 600 m deep, assuming an average velocity of 1550 m/s. The Linosa Graben is the southernmost analyzed basin, and it is the richest, among the analyzed basins, in magmatic intrusions, with a shallow manifestation in the northern rim (Fig. 11 b) attributed to Linosa II volcano (location in
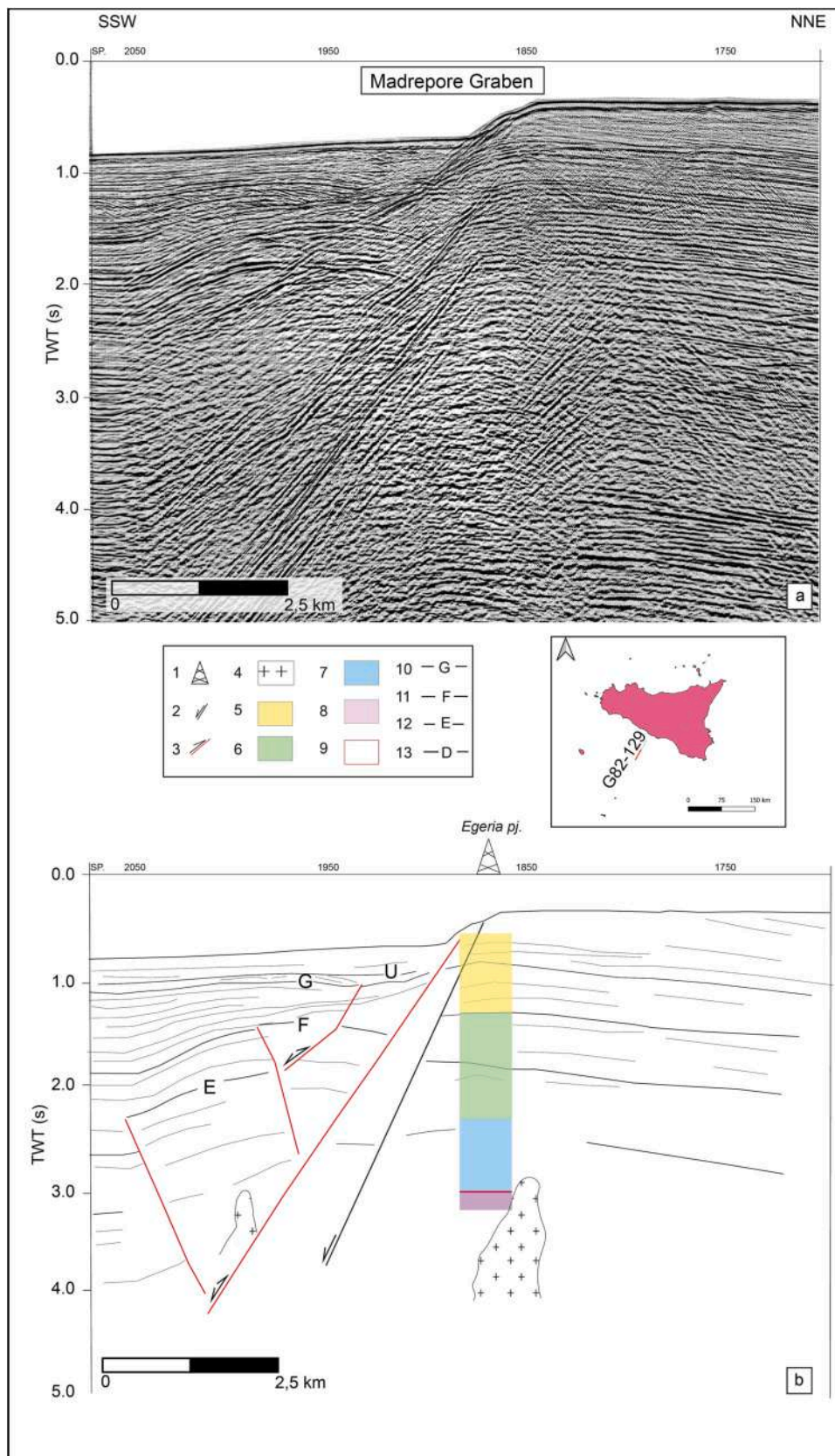
Fig. 8. (a) G82 129 seismic line showing Madrepore Graben structure (showed in Fig. 1), and (b) the relative line drawing and correlation with Egeria well-log. (c) G82 131 seismic line showing Falda di Gela (11 in Fig. 1), and (d) the relative line drawing and correlation with Palma well-log. 1: well location; 2: normal fault; 3: inverted fault; 4: crossing seismic line; 5: volcanic intrusion; 6: Plio-Pleistocene unit; 7: Eocene-Miocene unit; 8: Cretaceous units; 9: Jurassic unit; 10: Triassic unit; 11: magmatic levels; 12: possible magmatic intrusion; 13: 0.8 Ma unconformity; 14: 1.2 Ma unconformity; 15: Base Gelasian; 16: Top Messinian Evaporites; 17: Top Oligocene unit; 18: Top Eocene unit; 19: Top Cretaceous unit.
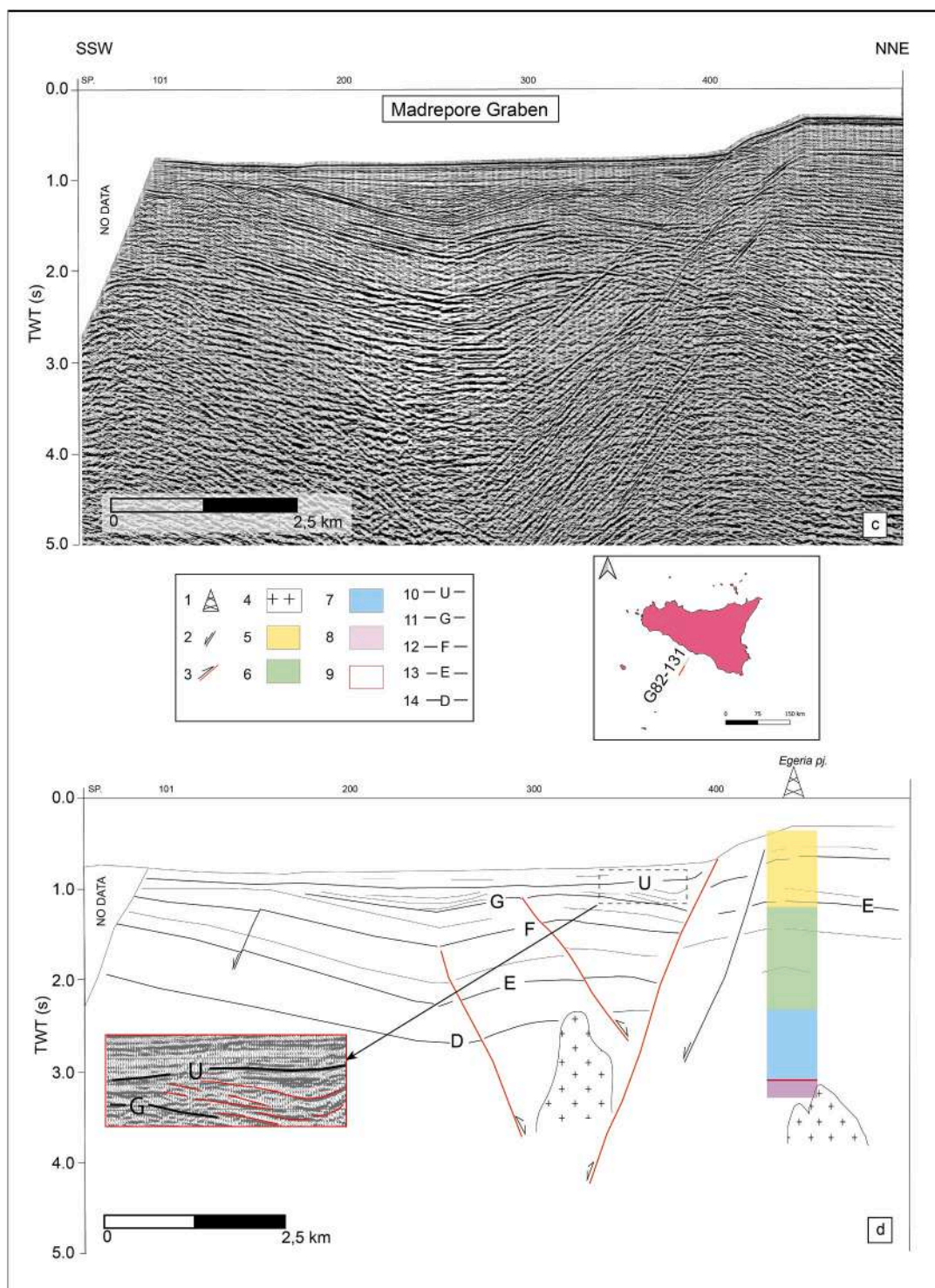
Fig. 8. (*continued*).

An extensional phase is detected by the *syn*-rift geometry of the unit between U1 and U2 in both MS 119 and CROP M24 seismic lines (Figs. 4, 11). The internal geometry of the Linosa Graben also shows the presence of a rollover anticline that involves the G and F horizons (Fig. 11 b). Even in this graben, a positive inversion shortens the rollover anticline which appears sealed by the U3 unconformity. In a similar way to the Madrepore Graben, the northern edge of the Linosa Graben is affected by a normal fault reaching the seafloor in the MS 119 (Fig. 11 b) but not in the M24, where instead a folded seafloor creates a positive relief of ∼400 m. This necessarily implies that within the Linosa Graben,

there is a local variation of the deformation in a few km of distance.

5. Discussion

5.1. Timing of the observed deformation phases

The seismo-stratigraphic interpretation allowed us to identify the chronology of the deformations occurred in an N-S-oriented band in the Sicily Channel. For the Madrepore, Malta, Linosa Graben, and the Linosa Plateau, the ages of the deformation stages have been derived by
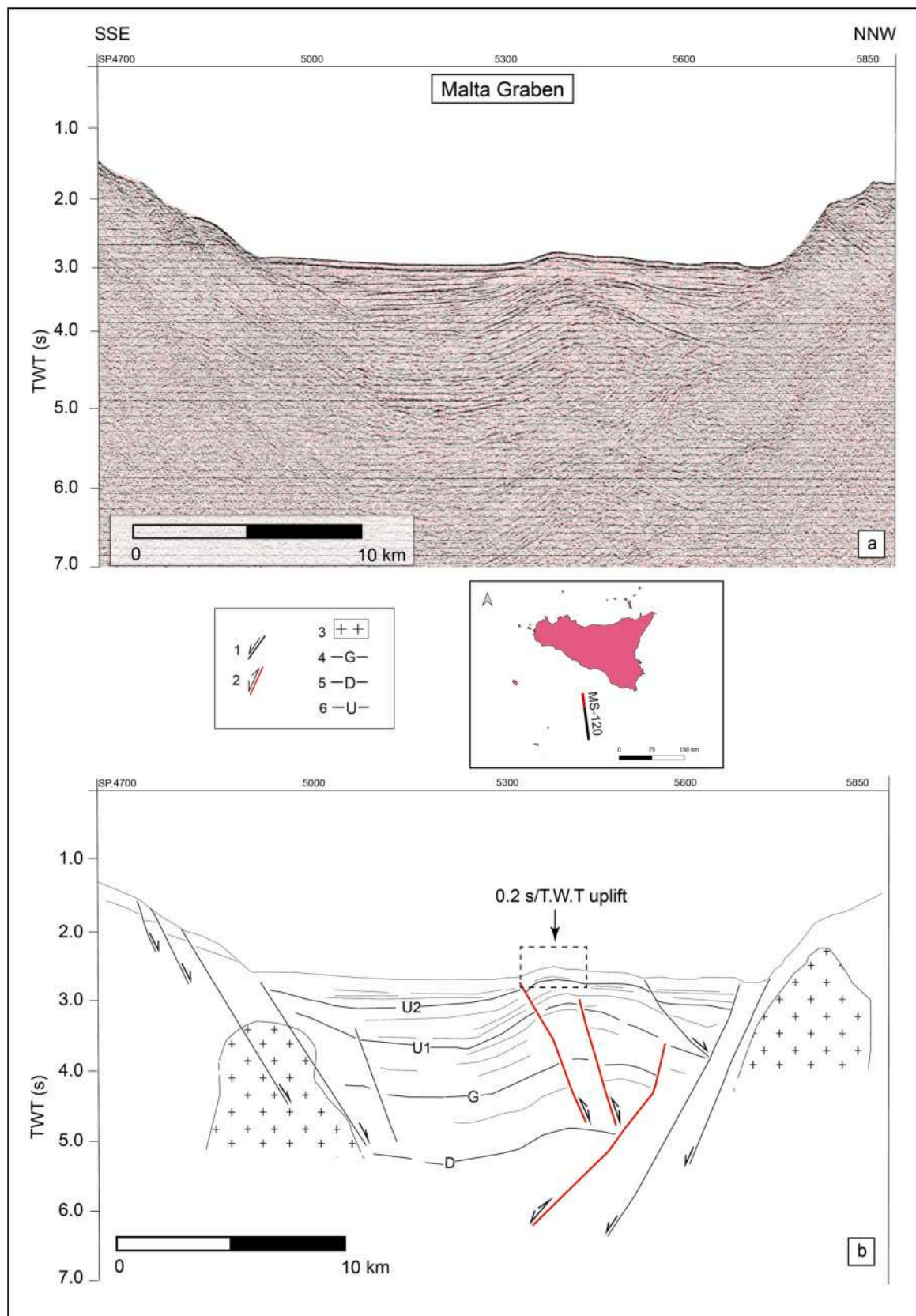
Fig. 9. (a) MS 120 line showing a positive relief of the seafloor in correspondence of Malta Graben (showed in Fig. 1), with (b) relative line drawing. The positive relief is absent in the (c) MS 119 seismic line and in the relative line drawing (d). Fig. 9 (e) shows a model of the positive inversion highlighted in Fig. 8 (b). 1: normal fault; 2: inverted fault; 3: volcanic intrusion; 4: Top Messinian Evaporites; 5: Top Cretaceous unit; 6: unconformity surface.
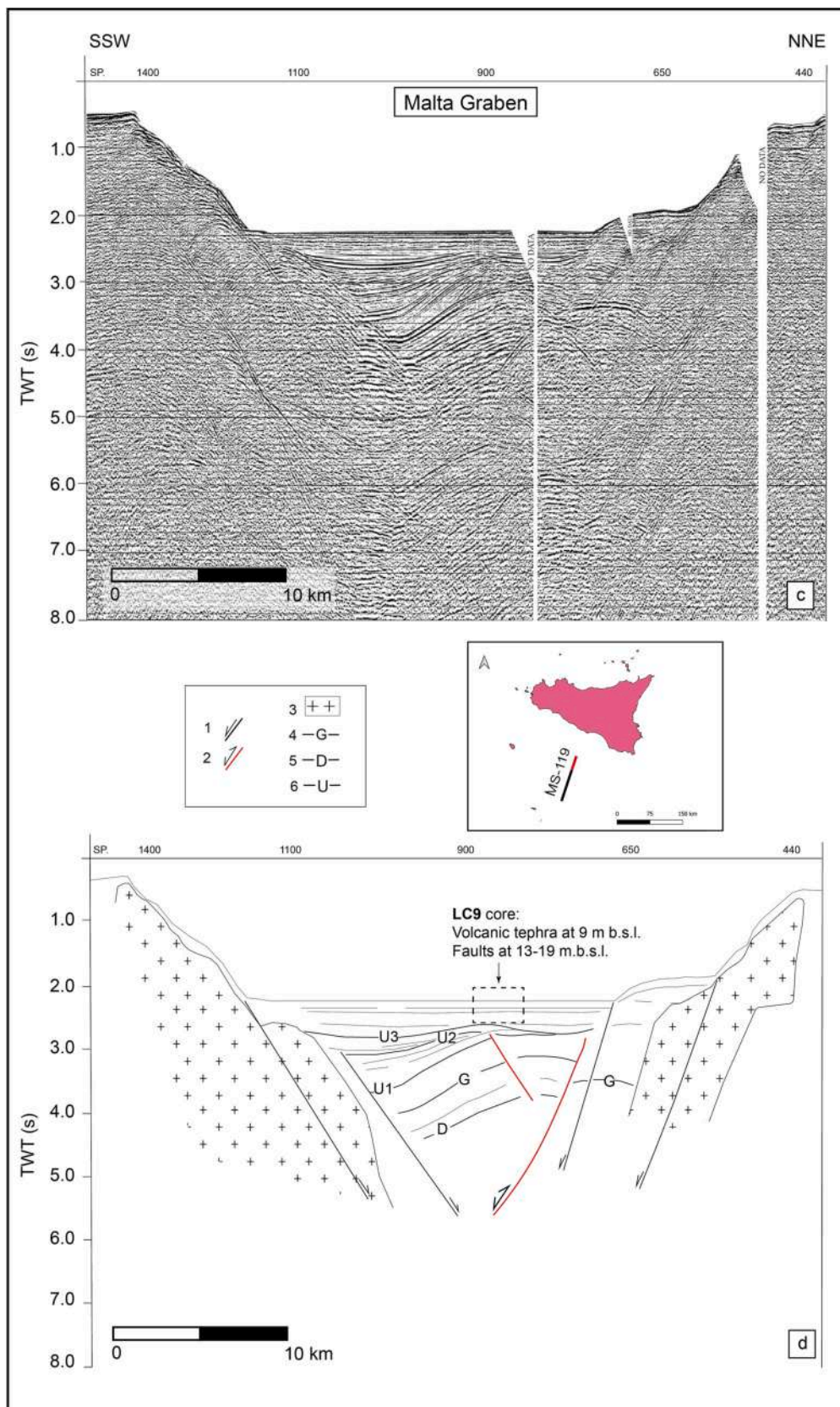
Fig. 9. (*continued*).

calculating the sedimentation rates for each level (Table 4) and by seismo-stratigraphic interpretation and well-tie. New constraints on the evolution of the different sectors investigated are presented below:

(a) Gela Thrust System: according to the Palma well-log analysis (Fig. 3), it involves deposits from the Paleogene to the Quaternary period. The seismo-stratigraphic analysis highlighted three main
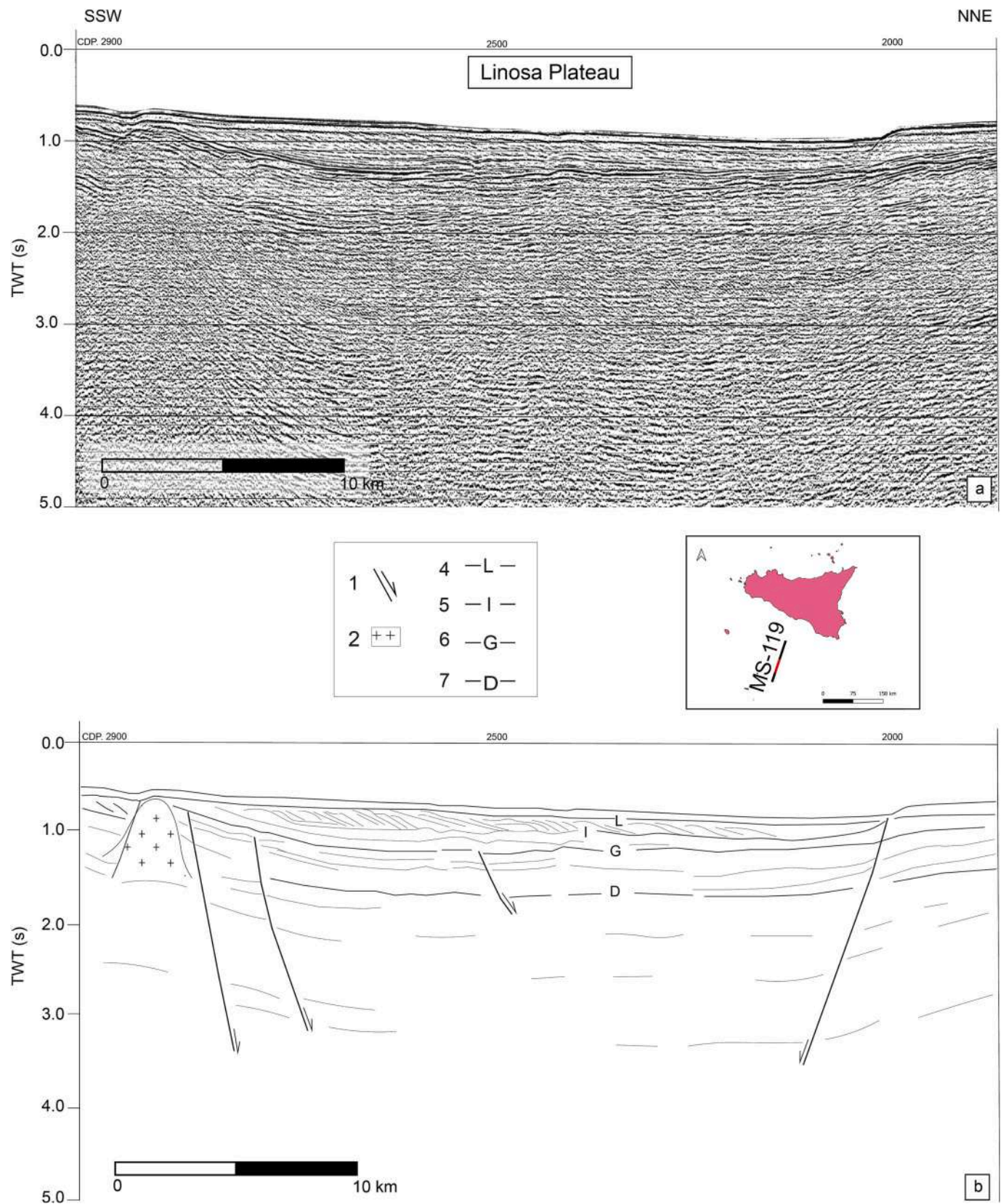
Fig. 10. (a) MS 119 seismic line showing prograding wedges in the Linosa Plateau and (b) relative line drawing. 1: normal fault; 2: volcanic intrusion; 3: 0.8 Ma unconformity; 4: 1.2 Ma unconformity; 5: Top Messinian Evaporites; 6: Top Cretaceous unit.
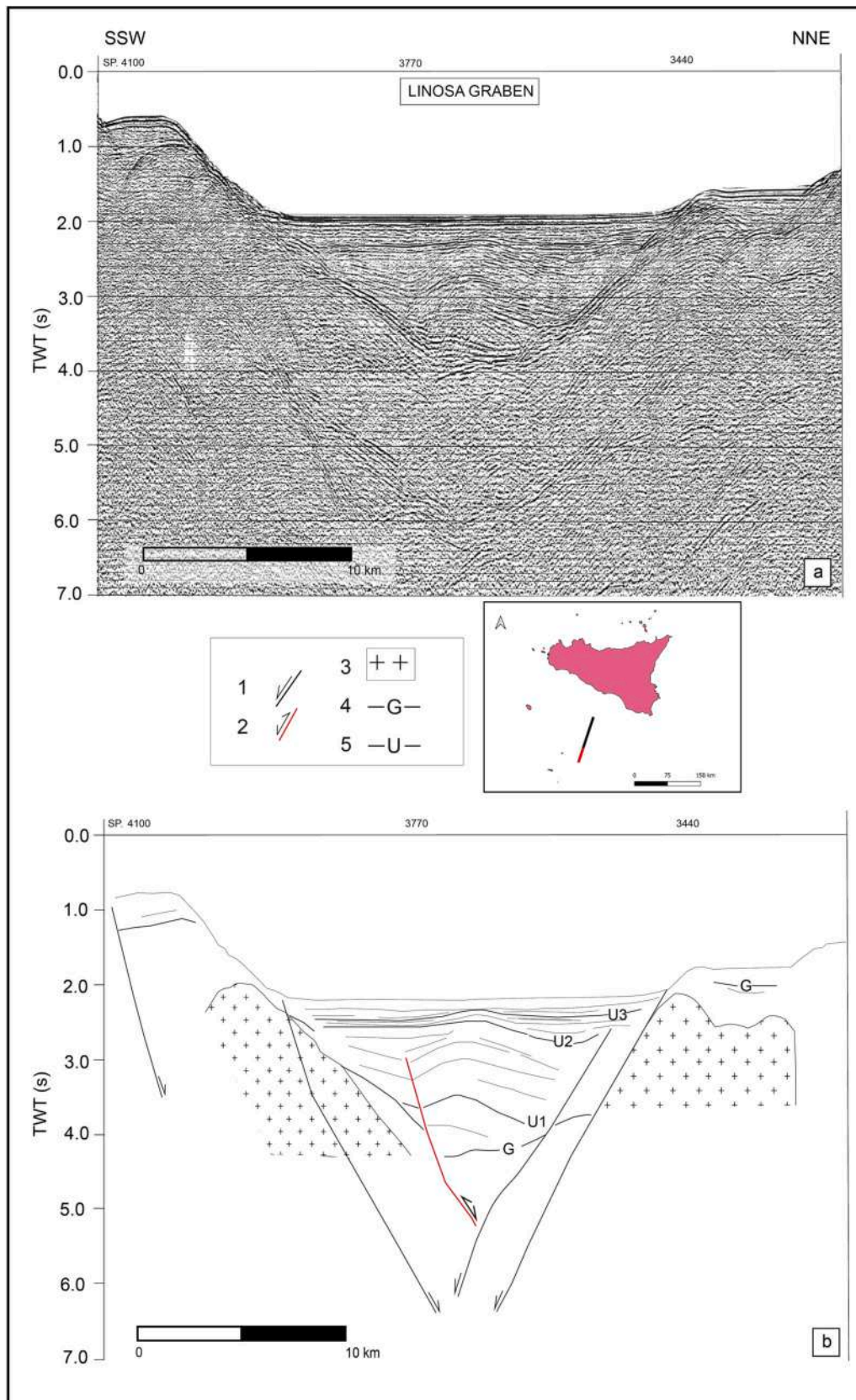
Fig. 11. (a) MS 119 seismic line the Linosa Graben (showed in Fig. 1) and (b) relative line drawing. 1: normal fault; 2: inverted fault; 3: volcanic intrusion; 4: Top Messinian Evaporites; 5: unconformity surface.

Table 4

Obtained sedimentation rate and age of main deformation events detected in Malta, Linosa and Madrepore Graben.

Line	Process	Thickness (s)	Thickness (mm)	Age (Ma)		Sedimentation rate	Area
MS-119	Extension (Seabed)	0,4	400,000	0,03	Calabrian-Chibanian		
	Inversion (top U3)	0,15	150,000	1,23	Calabrian	0,3 mm/yr	
	Extension (top U2)	0,8	800,000	1,63	Calabrian		
	Post-Messinian (top U1)	0,4	440,000	4,03	Zanclean		
MS-120	Inversion (top U3)	0,3	300,000	0,33	Chibanian		Malta Graben
	Extension (top U2)	0,6	660,000	1,33	Calabrian	0,4 mm/yr	
	Post-Messinian (top U1)	0,6	660,000	3,33	Piacenzian		
M24	Extension (seabed)	0,4	400,000	0,03	Calabrian-Chibanian		
	Inversion (top U3)	0,2	200,000	1,28	Calabrian	0,3 mm/yr	
	Extension (top U2)	0,5	500,000	1,83	Gelasian-Calabrian		
	Post-Messinian (top U1)	0,4	440,000	3,93	Zanclean		
M24	Inversion (Seabed)	0,3	300,000	0,04	recent		
	Extension (top U2)	0,35	385,000	1,34	Calabrian	0,24 mm/yr	
	Post-Messinian (top U1)	0,5	550,000	2,94	Piacenzian		
MS-119	Extension (Seabed)	0,3	300,000	0,03	Chibanian		Linosa Graben
	Inversion (top U3)	0,2	200,000	0,86	Calabrian	0,36 mm/yr	
	Extension (top U2)	0,9	990,000	1,41	Calabrian		
	Post-Messinian (top U1)	0,4	440,000	4,11	Zanclean		
G82–131	Inversion (Top U)	0,16	160,000	3,13	Piacenzian	0,7 mm/yr	Madrepore Graben

unconformity surfaces (H, I, L) that have been attributed to the main stages of deformation, respectively Zanclean (5.33 Ma), Piacenzian (3.6 Ma) and top of Calabrian (0.8 Ma), in agreement with literature data (Catalano et al., 1993; Cavallaro et al., 2017). Since the wedge appears sealed by 0.8 Ma unconformity (Horizon L) we suggest that its advancement is no longer active, in agreement with Di Stefano et al. (1993a)'s interpretation.

(b) Madrepore Graben: in the Madrepore Graben a Zanclean (5.33 Ma) extensional phase has been identified on the basis of the Horizon G displacement, dated back to the Messinian through the well-tie analysis. The observed *syn*-inversion deposits (Fig. 8 d) have been dated back to Piacenzian (3.13 Ma). The timing has been estimated considering 0.7 mm/yr of sedimentation rate for the units between G and U horizons, while the sedimentation rate was obtained by considering the maximum thickness of the units overlying the Messinian deposits (Horizon G) (Table 4). A third event of a recent, renewed, extensional phase (Post Piacenzian) was identified by a seafloor displacement (Fig. 8 a-d).

(c) Malta Graben: we identified three different deformation phases (U1-U3) (Fig. 9 b, d, e). The ages have been obtained by different sedimentation rates for each seismic line (M24, MS-120, MS-119) which consider the maximum thickness of the units overlying the post-Messinian deposits (Horizon G), dated back to 5.33 Ma (Table 4). The younger extensional event (between U1 and U2) has resulted to be: Piacenzian-Calabrian (3.33–1.33 Ma) in the MS-120 (using a sedimentation rate of 0.4 mm/yr); Zanclean-Calabrian (on average 3.9–1.7 Ma) in the M24 and MS-119, assuming a sedimentation rate of 0.33 mm/yr (Table 4). The second identified event (U2-U3) is an inversion phase that, with a sedimentation rate of ~0.35 mm/yr, has been dated in MS-119 and M24 to the upper Calabrian (1.2 Ma) (Table 3). The followed renewed extension is testified only in the M24 and MS-119 by recent normal faults intersecting the seafloor. Instead, the MS-120 shows a positive relief affecting the seabed which is uplifted at least 500 m high (Fig. 9 a, b); this implies that a contractional phase was or is still active in recent times and is mainly localized in the central Malta Graben.

(d) Linosa Plateau: according to the seismo-stratigraphic interpretation, the post-Messinian units appear affected by several normal faults that cause a moderate bending of the whole plateau (Fig. 10 b). This implies that an extensional phase took place during the deposition of the Messinian unit. These are covered by the 1.2 Ma unconformity (horizon I) and are overlaid by a series of pro-grading wedges topped by the 0.8 Ma unconformity (horizon L) (Fig. 10 b).

(e) Linosa Graben: an extensional phase is detected by the syn-rift deposits between U1 and U2 in both MS 119 and CROP M24 seismic lines (Figs. 4, 11). This event has been dated from Zanclean (4.11 Ma) to Calabrian (1.41 Ma) in the MS 119, assuming a sedimentation rate of 0.36 mm/yr; while in the M24 has been dated to Piacenzian (2.94 Ma)-Calabrian (1.34 Ma) (Table 3). The internal geometry of the Linosa Graben also shows the presence of a rollover anticline that involves the Messinian and Post-Messinian deposits (Fig. 11 b). Even in this graben, in the MS-119, a positive inversion shortens the rollover anticline which appears sealed by the U3 unconformity dated to upper Calabrian (0.86 Ma) (assuming a sedimentation rate of 0.24–0.36 mm/yr) (Table 3). While, in the M24, the inversion affects the seabed, which creates a positive relief of ~400 m, suggesting a more recent age. In a similar way to the Madrepore Graben, the northern edge of the Linosa Graben is affected, in the MS-119, by a normal fault reaching the seafloor suggesting a post-Calabrian deformation (Fig. 11 b). This necessarily implies that within the Linosa Graben, there is a local variation of the deformation in a few km of distance.

5.2. Magmatic intrusions

Several magmatic intrusions have been detected in the sallow layers, some of which have been calibrated with well-logs data (Egeria and Riccio Sud) (Fig. 8) and sampling (e.g. LC9 for Malta Graben). Shallow volcanic intrusions have been recognized in the seismic lines along Malta Graben and Linosa Graben, where there are also recorded outcropping volcanoes (Figs. 9 a-d, 11). In the deep layers, in correspondence with several Moho's interruptions, we observed the presence of diffraction hyperbolae causing signal anomalies linked to deep-origin fluids rising (Figs. 4, 12). This is suggested by the associated upwards occurrence of numerous volcanic bodies in the whole area, such as, for example, the Linosa II volcano, whose edifice outcrops at the rims of the Linosa graben (Fig. 11). Near Malta Graben, there is no gravimetric anomaly detected (Della Vedova et al., 1987), but it cannot be excluded an absence of a Moho's rising since the evidence of volcanic manifestations. Since the magmatic manifestations are concentrated along the main graben's margins, we suggest a relationship between extension and magmatism.

5.3. Constraints on the geodynamic evolution of the Sicily Channel

The response of continental forelands to subduction/collision is a widely investigated topic in the Mediterranean region (Maesano et al.,
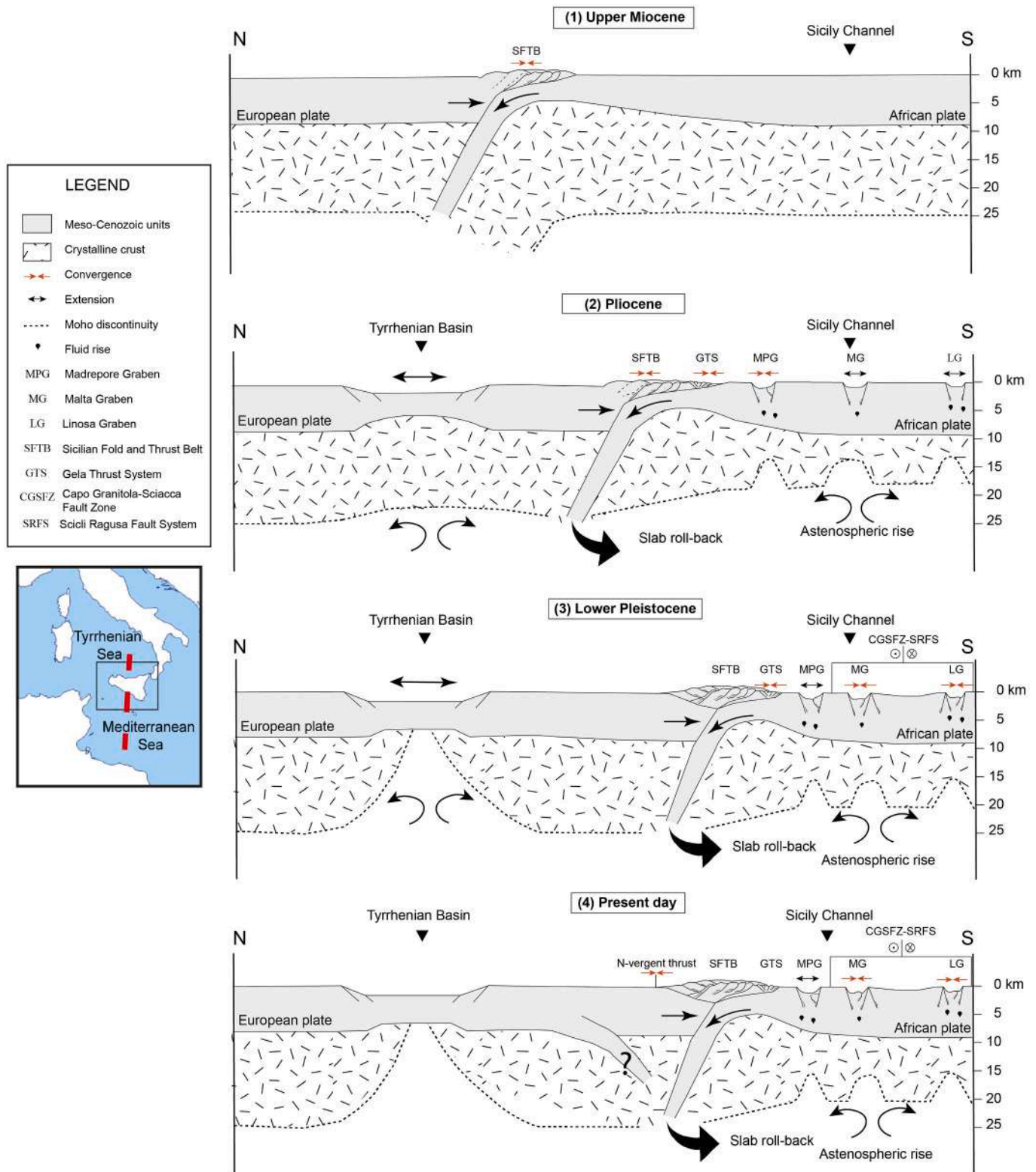
Fig. 12. Schematic representation showing the events that occurred in the Sicily Channel from Lower Pliocene to Present day after the slab roll-back of the African plate (modified after Argnani, 1990). In the bottom left corner is the rough location (red line) of the model. (For interpretation of the references to colour in this figure legend, the reader is referred to the web version of this article.)

2020). As already known by literature, and as confirmed by our seismic interpretation, the Sicily Channel is characterized by both extensional and contractional deformation. This is a typical feature of the Central Mediterranean region, such as for the nearby southern Adria plate, whose evolution since the late Neogene is characterized by extensional and compressional/transpressional pulses related to the alternation/coexistence of different tectonic processes (Chizzini et al., 2022).

However, the processes related to these deformation phases that affected our Sicilian foreland study area are still poorly defined, as well as how they acted during the geological time.
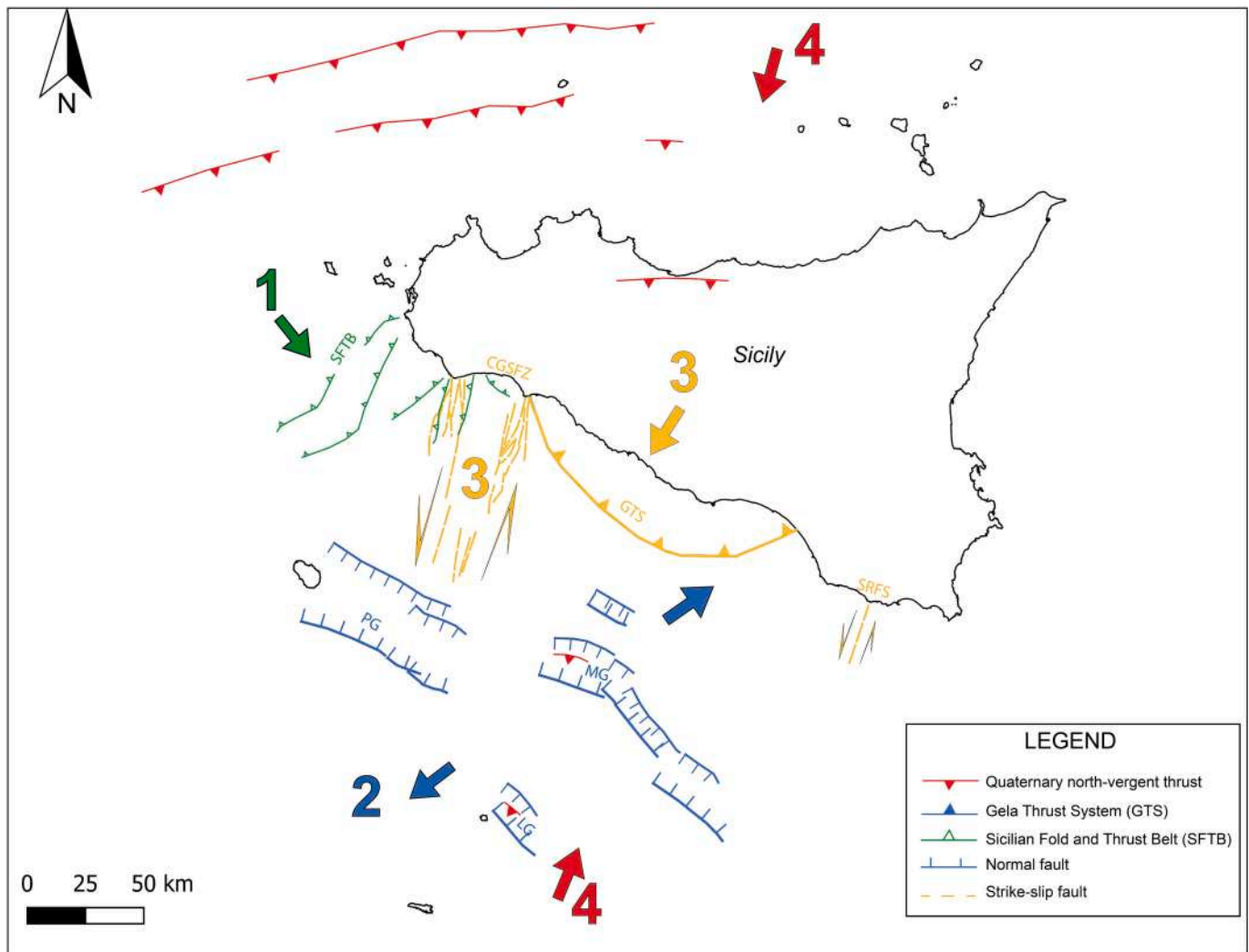
Fig. 13. Simplified plan representation of tectonic phases occurred in the Sicily Channel from the Late Miocene onwards. PG: Pantelleria Graben; MG: Malta Graben; LG: Linosa Graben; CGSFZ: Capo Granitola-Sciacca Fault Zone; SRFS: Scicly Ragusa Fault System.

In this section, we aim to discuss the relation of the observed extensional and contractional deformation with the regional geodynamic setting. We propose the following sequence of four tectonic events and main driving forces (Figs. 12, 13) as follows:

1. In the Upper Miocene, a regional contractional deformation occurred due to the convergence between Africa and Europe (Bellon & Letouzey, 1977; Dercourt et al., 1986; Dewey et al., 1989) producing the collisional Sicilian Fold and Thrust Belt (SFTB) and the Ionian-Tyrrhenian arc-trench complex (Sulli et al., 2021) (Figs. 12, 13).

2. In the Lower Pliocene, the foreland area of the African Plate, localized in the Sicily Channel, has been subject to a NW-SE oriented extension since 5.33 Ma ago (Zanclean) (Figs. 12, 13). The opening of the Pantelleria, Linosa and Malta grabens took place, potentially with a dextral strike-slip component (Catalano et al., 2009), especially in Malta and Linosa grabens. The extension was accompanied by changes in the asthenospheric flows, which led to the Moho (and magma) rising detected in the M24 seismic line under the main grabens and accompanied by local volcanic manifestation along the grabens' margins (Figs. 4, 12 b). These events could be related to the fast slab retreat of the Calabrian Arc (Faccenna et al., 2001a, 2001b), potential slab tearing (Arab et al. (2020) and the independent motion and rotation of the Adriatic Plate relative to Africa and Europe (Le

Breton et al., 2017). This is also supported by GPS data, which shows that the Africa-Europe convergence rate decreased by about 25–55% (Calais et al., 2003; Meccariello et al., 2017; Palano et al., 2020) from Oligocene to the present. Moreover, in the last 3 Ma, the African Plate rotates counterclockwise 20° relative to Eurasia, and Adria rotates 5°+/− 3° counterclockwise relative to Europe in the last 20 Ma (Dewey et al., 1989; Torelli et al., 1995; Calais et al., 2003; Le Breton et al., 2017). This caused a divergence between Africa and Adria of about 60 km, which seems to be accommodated by extension in the Sicily Channel (Le Breton et al., 2017).

3. In the Lower-Upper Pliocene, the Gela Thrust System (GTS) advance induced a positive reactivation phase in the Madrepore Graben (Fig. 12) dated to the Piacenzian age (3.13 Ma), which is in agreement with the first stage of advancement of the GTS dated by , and with the ages of tectonic reactivation detected by Cavallaro et al. (2017) and Civile et al. (2021) in the same area.

   In the Lower Pleistocene, the last stage of advancement of the GTS is recorded at 0.8 Ma (upper Calabrian), in accordance with the seismostratigraphic interpretation of Cavallaro et al. (2017). At this stage, the Madrepore graben returns to register an extensional phase, no longer subjected to the compression given by the GTS advancement. However, an inversion of previously formed normal faults occurred between 1.8 and 0.7 Ma (Calabrian) and is registered in the Malta and Linosa graben (in line also with Civile et al., 2021), which

after 0.7 Ma, (upper Calabrian) show again an extensional phase. Contemporaneously, a transpressive activity of the lithospheric discontinuities CGSFZ and SRFS is registered (Civile et al., 2021), probably responsible for the inversion and contraction deformation observed in the grabens.

4. Today, conversely to other studies, a recent inversion has been detected in the Malta and Linosa Grabens, not caused by the advance of the Gela Thrust System (no longer active) but most likely caused by a response to a possible plate re-organization and change of subduction polarity (Sulli et al., 2021). A link between the recent positive inversions and the plate re-organization comes from a recent study (Sulli et al., 2021) on the Sicilian compressional structures. They identified a shift of the deformation to the north, from the Gela Thrust System to the inner sector in the southern Tyrrhenian Sea that is consistent with the recent theories of a change in the subduction polarity in the central Mediterranean orogens (Mauffret et al., 2004; Billi et al., 2011; Roure et al., 2012; Arab et al., 2016; Hamai et al., 2018; Sulli et al., 2021). We believe that this compressive stress field triggers the localized reactivations of pre-existing zones of weakness such as the extensional faults, especially in the Malta Graben but also in the Madrepore and Linosa Graben (Figs. 12, 13). This last stage is also accommodated by sinistral transcurrent zone (CGSFZ in particular), which today is seismically active and subdivides the Sicily Channel into a westward and eastward sector (Civile et al., 2021), as testified by focal mechanisms in the area (Fig. 1).

6. Conclusions

The comparative analysis of several seismic lines, reaching even the crustal structure, in addition to geodetic and literature data, allowed us to suggest that alternative extensional and contractional deformation located within the African Plate can be explained through the overlapping of different processes, as follows:

I. In the Upper Miocene a regional contractional deformation occurred due to the regional convergence between Africa and Europe producing the Sicilian Fold and Thrust Belt;

II. After the Messinian (post 5.33 Ma), in the Lower Pliocene, the fast rollback of the Calabrian slab caused a NW-SE oriented extensional phase that induced the formation of the main grabens;

III. This extensional phase appears partly contemporary with the advance of the Gela Thrust Front (GTS) that caused the Madrepore Graben positive reactivation in the Zanclean time (3.9 Ma). This is followed in the Lower Pleistocene, between 1.8 and 0.7 Ma (Calabrian), by a contractional phase, caused by the further activity of the GTS and onset of transpressive activity of the CGSFZ and SRFS, induced fault reactivations and inversion in Malta and Linosa Grabens;

IV. Today, the Malta Graben and Linosa Graben appear indeed affected by a recent contractional phase which caused positive reliefs of the seabed; this phase has been related to the potential change in the subduction polarity of the Africa plate suggested by geodetic and previous work in Sicily (Sulli et al., 2021). This recent plate re-organization seems not only to affect the northern part of Sicily and the southern Tyrrhenian Sea sectors but also the Sicily Channel.

We depict a tectonic setting in the Sicily Channel that is not the result of a simple stage of passive rifting. The Sicily Channel structural setting resulted indeed from the interplay of different processes which derive from the complex geodynamic system of the Central Mediterranean, especially from its subduction dynamics with the fast roll-back of the Calabrian Slab and subsequent potential slab tear and polarity switch north of Sicily.

Appendix A. Supplementary data

Supplementary materials to this article can be found online at https://doi.org/10.1016/j.tecto.2023.230019.

References

Agius, M.R., Magrini, F., Diaferia, G., Kästle, E.D., Cammarano, F., Faccenna, C., et al., 2022. Shear-velocity structure and dynamics beneath the Sicily Channel and surrounding regions of the Central Mediterranean inferred from seismic surface waves. Geochem. Geophys. Geosyst. 23 https://doi.org/10.1029/2022GC010394 e2022GC010394.

Aissi, M., Flovere, M., Würtz, M., 2015. Seamounts and seamount-like structures of and delamination of its continental lithosphere. Tectonics 31.

Andreetto, F., Aloisi, G., Raad, F., Heida, F., Flecker, R., Agiadi, K., Lofi, J., Blondel, S., Bulian, F., Camerlenghi, A., Caruso, A., Ebner, R., Garcia-Castellanos, D., Gaullier, V., Guibourdenche, L., Gvirtzman, Z., Hoyle, T.M., Meijer, P.T., Moneron, J., Sierro, F.J., Travan, G., Tzevahirtzian, A., Vasiliev, I., Krijgsman, W., 2021. Freshening of the Mediterranean Salt Giant: controversies and certainties around the terminal (Upper Gypsum and Lago-Mare) phases of the Messinian Salinity Crisis. Earth Sci. Rev. 216, 103577 https://doi.org/10.1016/j.earscirev.2021.103577.

Antonelli, M., Franciosi, R., Querci, A., Ronco, G., Vezzanini, F., 1988. Paleogeographic evolution and structural setting of the northern side of the Sicily Channel. In: Società Geologica Italiana, 74. Congresso Nazionale, Relazioni, pp. 79–86.

Arab, M., Rabineau, M., Bracene, R., D'everch'ere, J., Belhai, D., Roure, F., Marok, A., Bouyahiaoui, B., Granjeon, D., Andriessen, P., Sage, F., 2016. Tectono-sedimentary evolution of the Eastern Algerian margin and basin from seismic data and onshore-offshore correlation. Mar. Pet. Geol. 77, 1355–1375. https://doi.org/10.1016/j.marpetgeo.2016.08.021.

Arab, M., Maherssi, C., Granjeon, D., Roure, F., Dverchere, J., Cuilhe, L., Hassaim, M., Mouchot, N., Doublet, S., Khomi, S., 2020. On the origin and consequences of crustal-scale extension between Africa and Sicily since Late Miocene: insights from the Kaboudia area, western Pelagian Sea. Tectonophysics 795 (2020), 228565.

Argnani, A., 1990. The strait of Sicily Rift Zone: foreland deformation related to the evolution of a back-arc basin. J. Geodyn. 12, 312–331.

Argnani, A., 2009. Evolution of the southern Tyrrhenian slab tear and active tectonics along the western edge of the Tyrrhenian subducted slab. In: Van Hinsbergen, D.J.J., Edwards, M.A., Govers, R. (Eds.), Collision and the Collapse at the Africa-Arabia-Eurasia Subduction Zone. Geological Society London, Special Publication, 311, pp. 193–212.

Bally, A.W., 1983. Seismic Expression of Structural Styles: A Picture and Work Atlas. The American Association of Petroleum Geologists.

Basilone, L., 2009. Mesozoic tectono-sedimentary evolution of Rocca Busambra in western Sicily. Facies. 55, 115–135. https://doi.org/10.1007/s10347-008-0156-2.

Beccaluva, L., Colantoni, P., Savelli, C., Di Girolamo, P., 1981. Upper-Miocene submarine volcanism in the Strait of Sicily (Banco senza Nome). Bull. Volcanolog. 44 (3), 573–581.

Bellon, H., Letouzey, J.,1977. Volcanism related to plate tectonics in the western and eastern Mediterranean. *Structural History of the Mediterranean Basins.* Technip, Paris, pp. 165–184.

Billi, A., Faccenna, C., Bellier, O., Minelli, L., Neri, G., Piromallo, C., Presti, D., Scrocca, D., Serpelloni, E., 2011. Recent tectonic reorganization of the Nubia-Eurasia convergent boundary heading for the closure of the western Mediterranean. Bull. Soc. Géol. France 182 (4), 279–303.

Boccaletti, M., Cello, G., Tortorici, L., 1987. Transtensional tectonics in the Sicily Channel. J. Struct. Geol. 9 (7), pp. 869–876, 7.

Butler, R.W.H., Grasso, M., La Manna, F., 1992. Origin and deformation of the Neogene–recent Maghrebian foredeep at the Gela Nappe, SE Sicily. J. Geol. Soc. 1992 149 (4), 547–556. https://doi.org/10.1144/gsjgs.149.4.0547.

Butler, R.W.H., Lickorish, W.H., Grasso, M., Pedley, H.M., Ramberti, L., 1995. Tectonics and sequence stratigraphy in Messinian Basins, Sicily: constraints on the initiation and termination of the Mediterranean salinity crisis. Geol. Soc. Am. Bull. 107, 425–439.

Calais, E., Vergnolle, M., San'kov, V., Lukhnev, A., Miroshnitchenko, A., Amarjargal, S., De'verche're, J., 2003. GPS measurements of crustal deformation in the Baikal-Mongolia area (1994–2002): Implications for current kinematics of Asia. J. Geophys. Res. 108 (B10), 2501. https://doi.org/10.1029/2002JB002373.

Calò, M., Parisi, L., 2014. Evidence of a lithospheric fault zone in the Sicily Channel continental rift (southern Italy) from instrumental seismicity data. Geophys. J. Int. 199 (1) https://doi.org/10.1093/gji/ggu249. October Pages 219225.

Caracausi, A., Favara, R., Italiano, F., Nuccio, P.M., Paonita, A., Rizzo, A., 2005. Active geodynamics of the central Mediterranean Sea: Tensional tectonic evidences in western Sicily from mantle-derived helium. Geophys. Res. Lett. 32 (4).

Carminati, E., Doglioni, C., 2005. Mediterranean Tectonics. https://doi.org/10.1016/B0-12-369359-9/00135-0.

Casero, P., Cita, M.B., Croce, M., De Micheli, A., 1984. Tentativo di interpretazione evolutiva della scarpata di Malta basata su dati geologici e geofisici. Mem. Soc. Geol. It. 27, 235–253.

Catalano, R., Franchino, A., Merlini, S., Sulli, A., 2000. A crustal section from the Eastern Algerian basin to the Ionian ocean (Central Mediterranean). Mem. Soc. Geol. It. 71–85 (2000). 8 ff. 2 pl. f. t.

Catalano, R., Infuso, S., Sulli, A., 1993. The Pelagian Foreland and its northward foredeep. Plio-Pleistocene structural evolution. In: Max, M.D., Colantoni, P. (Eds.), Geological development of the Sicilian-Tunisian platform, Unesco report in Marine Science, 58, pp. 37–42.

Catalano, R., D'Argenio, B., 1982. Schema geologico della Sicilia. In: Catalano, R., D'Argenio, B. (Eds.), Guida alla geologia della Sicilia occidentale. — Soc. Geol. It., Palermo.

Catalano, S., De Guidi, G., Romagnoli, G., Torrisi, S., Tortorici, G., Tortorici, L., 2008. The migration of plate boundaries in SE Sicily: influence on the large-scale kinematic model of the African promontory in southern Italy. Tectonophysics 449 (1–4), 41–62.

Catalano, S., Guidi, De, Lanzafame, G., Monaco, C., Tortorici, L., 2009. Late Quaternary deformation on the island on Pantelleria: new constraints for the recent tectonic evolution of the Sicily Channel Rift (southern Italy). J. Geodyn. 48 (2), 75–82.

Catalano, R., Valenti, V., Albanese, C., Accaino, F., Sulli, A., Tinivella, U., Gasparo Morticelli, M., Zanolla, C., Giustiniani, M., 2013. Sicily's fold–thrust belt and slab roll-back: the SI. RI. PRO. seismic crustal transect. J. Geol. Soc. 170 (3), 451–464.

Cavallaro, D., Monaco, C., Polonia, A., Sulli, A., Di Stefano, A., 2017. Evidence of positive tectonic inversion in the north-central sector of the Sicily Channel (Central Mediterranean). Nat. Hazards 86 (Suppl. 2), 233–251. https://doi.org/10.1007/s11069-016-2515-6.

Cello, G., 1987. Structure and deformation processes in the Strait of Sicily "rift zone". Tectonophysics 141, 237–247.

Chizzini, N., Artoni, A., Torelli, L., Basso, J., Polonia, A., Gasperini, L., 2022. Tectono-stratigraphic evolution of the offshore Apulian Swell, a continental sliver between two converging orogens (Northern Ionian Sea, Central Mediterranean). Tectonophysics 839 (August). https://doi.org/10.1016/j.tecto.2022.229544.

Christensen, N.I., Mooney, W.D., 1995. Seismic velocity structure and composition of the continental crust: a global view. J. Geophys. Res. Solid Earth 100, 9761–9788. https://doi.org/10.1029/95JB00259.

Civile, D., Lodolo, E., Tortorici, L., Lanzafame, G., Brancolini, G., 2008. Relationships between magmatism and tectonics in a continental rift: The Pantelleria Island region (Sicily Channel, Italy). Mar. Geol. 251 (1–2) https://doi.org/10.1016/j.margeo.2008.01.009. Pages 32-46, ISSN 0025–3227.

Civile, D., Lodolo, E., Accettella, D., Geletti, R., Ben-Avraham, Z., Deponte, M., Facchin, L., Ramella, R., Ro-meo, R., 2010. The Pantelleria graben (Sicily Channel, central Mediterranean): An example of intraplate 'passive' rift. Tectonophysics 490, 173–183. References.

Civile, D., Lodolo, E., Zecchin, M., 2015. The lost Adventure Archipelago (Sicilian Channel, Mediterranean Sea): morpho-bathymetry and late Quaternary palaeogeographic evolution. Glob. Planet. Chang. 125, 3647.

Civile, D., Lodolo, E., Accaino, F., Geletti, R., Schiattarella, M., Giustiniani, M., Fedorik, J., Zecchin, M., Zampa, L., 2018. Capo Granitola-Sciacca Fault Zone (Sicilian Channel, Central Mediterranean): Structure vs magmatism. Mar. Pet. Geol. 96, 627–644. ISSN 0264 8172,. https://doi.org/10.1016/j.marpetgeo.2018.05.016.

Civile, D., Brancolini, G., Lodolo, E., Forlin, E., Accaino, F., Zecchin, M., Brancatelli, G., 2021. Morphostructural setting and tectonic evolution of the Central Part of the Sicilian Channel (Central Mediterranean). Lithosphere 2021 (1), 1–24. https://doi.org/10.2113/2021/7866771.

Corti, G., Cuffaro, M., Innocenti, F., Manetti, P., 2006. Coexisting geodynamic processes in the Sicily Channel. Geol. Soc. Am. Spec. Pap. 409, 83–96.

D'Agostino, N., Selvaggi, G., 2004. Crustal motion along the Eurasia-Nubia plate boundary in the Calabrian Arc and Sicily and active extension in the Messina Straits from GPS measurements. J. Geophys. Res. 109, B11402 doi:10.1022004JB002998.

Della Vedova, B., Pellis, G., Corubolo, P., 1987. Evidenze termiche del rifting nel Canale di Sicilia. Atti 6° Convegno GNGTS. CNR Roma, pp. 687–698.

Dercourt, J.E.A., Zonenshain, L.P., Ricou, L.E., Kazmin, V.G., Le Pichon, X., Knipper, A.L., Grandjacquet, C., Sbortshikov, I.M., Geyssant, J., Lepvrier, C., Pechersky, D.H., Boulin, J., Sibuet, J.-C., Savostin, L.A., Sorokhtin, O., Westphal, M., Bazhenov, M.L., Lauer, J.P., Biju-Duval, B., 1986. Geological evolution of the Tethys belt from the Atlantic to the Pamirs since the Lias. Tectonophysics 123 (1–4), 241–315.

Devoti, R., Esposito, A., Pietrantonio, G., Pisani, A.R., Riguzzi, F., 2011. Evidence of large-scale deformation patterns from GPS data in the Italian subduction boundary. Earth Planet. Sci. Lett. 311, 230–241. https://doi.org/10.1016/j.epsl.2011.09.034.

Dewey, J.F., Helman, M.L., Turco, E., Hutton, D.H.W., Knott, S.D., 1989. Kinematics of.

Di Stefano, E., Infuso, F., Scarantino, S., 1993a. Plio-Pleistocene sequence stratigraphy of south western offshore Sicily from well-logs and seismic sections in a high-resolution calcareous plankton biostratigraphic framework. In: Max, M.D., Colantoni, P. (Eds.), Geological DEvelopment of the Sicilian-Tunisian Platform: Unesco Report in Marine Science 58, 105–110.

Faccenna, C., Funiciello, F., Giardini, D., Lucente, P., 2001a. History of subduction and back-arc extension in the Central Mediterranean. Geophys. J. Int. 145, 809–820.

Faccenna, C., Funiciello, F., Giardini, D., Lucente, P., 2001b. Episodic back-arc extension during restricted mantle convection in the Central Mediterranean. Earth Planet. Sci. Lett. 187, 105–116.

Ferranti, L., Pepe, F., Barreca, G., Meccariello, M., Monaco, C., 2019. Multi-temporal tectonic evolution of Capo Granitola and Sciacca foreland transcurrent faults (Sicily channel). Tectonophysics 765 (January), 187–204. https://doi.org/10.1016/j.tecto.2019.05.002.

Finetti, I.R., 1984. Geophysical study of the Sicily Channel Rift Zone. Boll. Geofis. Teor. Appl. 26, 3–28.

Finetti, I.R., Del Ben, A., 2005. Crustal tectono-stratigraphy of the Ionian Sea from new integrated CROP seismic data. In: Finetti, I.R. (Ed.), Elsevier special volumeCrop Project Project – Deep Seismic exploration of the Central Mediterranean and Italy, pp. 447–470.

Finetti, I., Morelli, C., 1973a. Esplorazione sismica per riflessione dei Golfi di Napoli e Pozzuoli. Boll. Geofis. Teor. Appl. 16, 175–222.

Finetti, I., Morelli, C., 1973b. Geophysical exploration of the Mediterranean Sea. Boll. Geofis. Teor. Appl. 15, 263–341.

Ghielmi, M., Amore, M., Bolla, E., Carubelli, P., Knezaureki, G., Serraino, C., 2012. The Pliocene to Pleistocene Succession of the Hyblean Foredeep (Sicily, Italy). AAPG Search and Discovery.

Govers, R., Wortel, M.J.R., 2005. Lithosphere tearing at STEP faults: response to edge of subduction zones. Earth Planet. Sci. Lett. 236, 505–523. https://doi.org/10.1016/j.epsl.2005.03.022.

Grasso, M., Reuther, C.D., 1988. The western margin of the Hyblean Plateau: a neotectonic transform system on the SE Sicilian foreland. Ann. Tecton. 2 (2), 107–120.

Grasso, M., Torelli, L., 1999. Cretaceous-Paleogene sedimentation patterns and structural evolution of the Tunisian shelf, offshore the Pelagian Islands (Central Mediterranean). Tectonophysics 315 (1999), 235–250.

Hamai, L., Petit, C., Le Porhiet, L., Yelles-Chaouche, A., D'everch'ere, J., Beslier, M.O., Abtout, A., 2018. Towards subduction inception along the inverted North African margin of Algeria? Insights from thermo-mechanical models. Earth Planet. Sci. Lett. 501, 13–23.

Handy, M.R., Schmid, S.M., Bousquet, R., Kissling, E., Bernoulli, D., 2010. Reconciling plate-tectonic reconstructions with the geological-geophysical record of spreading and subduction in the Alps. Earth Sci. Rev. 102, 121–158.

Haq, B., Gorini, C., Baur, J., Moneron, J., Rubino, J.-L., 2020. Deep Mediterranean's Messinian evaporite giant: how much salt? Glob. Planet. Chang. 184, 103052. ISSN 0921-8181. https://doi.org/10.1016/j.gloplacha.2019.103052.

Hart, B.S., 2010. Introduction to Seismic Interpretation, AAPG Discovery Series No. 16.

Hollenstein, C., Kahle, H.-G., Geiger, A., Jenny, S., Goes, S., Giardini, D., 2003. New GPS constraints on the Africa-Eurasia plate boundary zone in southern Italy. Geophys. Res. Lett. 30 (18), 4. https://doi.org/10.1029/2003GL017554.

Hsü, K.J., Cita, M.B., Ryan, W.B.F., 1973. The origin of the Mediterranean evaporites. In: Ryan, W.B.F., Hsü, K.J., et al. (Eds.), Initial Rep. Deep Sea Drill. Prog, vol. 13. U.S. Govt. Printing Office, Washington, DC, pp. 1203–1231.

ISIDe Working Group, 2007. Italian Seismological Instrumental and Parametric Database (ISIDe) doi.org/10.13127/ISIDE.

Jongsma, D., Van Hinte, J.E., Woodside, J.M., 1985. Geologic structure and neotectonics of the North African Continental Margin south of Sicily. Mar. Pet. Geol. 2, 156–179.

Lanzafame, G., Rossi, P.L., Tranne, C.A., Lanti, E., 1994. Carta geologica dell'isola di Linosa, scale 1:5,000. SELCA, Firenze.

Le Breton, E., Handy, M.R., Molli, G., Ustaszewski, K., 2017. Post-20 Ma motion of the Adriatic plate: New constraints from surrounding Orogens and implications for crust-mantle decoupling. Tectonics 36, 3135–3154. https://doi.org/10.1002/2016TC004443.

Le Breton, E., Brune, S., Ustaszewski, K., Zahirovic, S., Seton, M., Müller, R.D., 2021. Kinematics and extent of the Piemont–Liguria Basin – implications for subduction processes in the Alps. Solid Earth 12, 885–913. https://doi.org/10.5194/se-12-885-2021.

Lickorish, W., Grasso, M., Butler, R., Argnani, A., Maniscalco, R., 1999. Structural styles and regional tectonic setting of the "Gela Nappe" and frontal part of the Maghrebian thrust belt in Sicily. Tectonics 18 (4), 655–668.

Lodolo, E., Civile, D., Zanolla, C., 2012. Magnetic signature of the Sicily Channel volcanism. Mar. Geophys. Res. 33 (2012), 33–44 doi:10.1007/s11001-011-9144-y.

Lodolo E., Civile D., Zecchin M: Zampa L. S., Accaino F., 2019. A series of volcanic edifices discovered a few kilometers off the coast of SW Sicily, Mar. Geol., vol. 416, 105999, ISSN 0025–3227, doi:https://doi.org/10.1016/j.margeo.2019.105999.

Lofi, J., Déverchère, J., Gaullier, V., Illet, H., Guennoc, P., Gorini, C., Loncke, L., Maillard, A., Sage, F., Thinon, I., 2011. Seismic Atlas of the Messinian Salinity Crisis Markers in the Offshore Mediterranean Domain. CCGM & Mém. Soc. géol. Fr., n.s.

Maesano, F.E., Volpi, V., Civile, D., Basili, R., Conti, A., Tiberti, M.M., Accettella, D., Conte, R., Zgur, F., Rossi, G., 2020. Active Extension in a Foreland Trapped between two Contractional chains: the South Apulia Fault System (SAFS). Tectonics 39 (7). https://doi.org/10.1029/2020TC006116.

Mauffret, A., Frizon de Lamotte, D., Lallemant, S., Gorini, C., Maillard, A., 2004. E–W opening of the Algerian Basin (Western Mediterranean). Terra Nova 16 (5), 257–264. https://doi.org/10.1111/j.1365-3121.2004 00559.x.

Meccariello, M., Ferranti, L., Barreca, G., Palano, M., 2017. New insights on the tectonics of the Lampedusa Plateau from the integration of offshore, onland and space geodetic data. Ital. J. Geosci. 136, 1–42. https://doi.org/10.3301/IJG.2017.02.

Micallef, A., Spatola, D., Caracausi, A., Italiano, F., Barreca, G., D'Amico, S., Petronio, L., Coren, F., Facchin, L., Blanos, R., Pavan, A., Paganini, P., Taviani, M., 2019. Active degassing across the Maltese Islands (Mediterranean Sea) and implications for its neotectonics. Mar. Pet. Geol. 104, 2019. Pages 361-374, ISSN 0264–8172. https://doi.org/10.1016/j.marpetgeo.2019.03.033.

Mitchum, R.M., Vail, P.R., Thompson, S., 1977. Applications to hydrocarbon exploration, Seismic stratigraphy and global changes of sea-level, part 2: the depositional sequence as a basic unit for stratigraphic analysis. In: Seismic Stratigraphy—American Association of Petroleum Geologists, Memoir, ed Payton C. E, 26, pp. 53–62.

Palano, M., Ferranti, L., Monaco, C., Mattia, M., Aloisi, M., Bruno, V., Cannavò, F., Siligato, G., 2012. GPS velocity and strain fields in Sicily and southern Calabria, Italy: Updated geodetic constraints on tectonic block interaction in the Central Mediterranean. J. Geophys. Res. 117, B07401. https://doi.org/10.1029/2012JB009254.

Palano, M., Ursino, A., Spampinato, S., Sparacino, F., Polonia, A., Gasperini, L., 2020. Crustal deformation, active tectonics, and seismic potential in the Sicily Channel (Central Mediterranean), along the Nubia–Eurasia plate boundary. Sci. Rep. (2020) 10, 21238.

Reeder, M., Rothwell, G., Stow, D., 2002. The Sicilian gateway: anatomy of the deep-water connection between East and West Mediterranean basins. Geol. Soc. Lond. Mem. 22, 171–189. https://doi.org/10.1144/GSL.MEM.2002.022.01.13.

Reuther, C.D., Eisbacher, C.H., 1985. Pantelleria rift: crustal extension in a convergent intraplate setting. Geol. Rundsch. 74, 58,55 87.

Romagnoli, C., Belvisi, V., Innangi, S., Di Martino, G., Tonielli, R., 2020. New insights on the evolution of the Linosa volcano (Sicily Channel) from the study of its submarine portions. Mar. Geol. 419, 106060.

Rosenbaum, G., Gasparon, M., Lucente, F.P., Peccerillo, A., Miller, M.S., 2008. Kinematics of Slab Tear Faults during Subduction Segmentation and Implications for Italian.

Roure, F., Casero, P., Addoum, B., 2012. Alpine inversion of the North African margin and delamination of its continental lithosphere. Tectonics 31, tc3006. https://doi.org/10.1029/2011tc002989, 2012tc30061of28.

Roveri, M., Flecker, R., Krijgsman, W., Lofi, J., Lugli, S., Manzi, V., Sierro, F.J., Bertini, A., Camerlenghi, A., De Lange, G., Govers, R., Hilgen, F.J., Hübscher, C., Th Meijer, P., Stoica, M., 2014. The Messinian Salinity Crisis: Past and future of a great challenge for marine sciences. Mar. Geol. 352 https://doi.org/10.1016/j.margeo.2014.02.002, 2014, Pages 25-58, ISSN 0025–3227.

Sandwell, D.T., Garcia, E., Soofi, K., Wessel, P., Smith, W.H.F., 2013. Towards 1 mGal Global Marine Gravity from CryoSat-2, Envisat, and Jason-1. Lead. Edge 32 (8), 892899. https://doi.org/10.1190/tle32080892.1.

Scarascia, S., Lozej, A., Cassinis, R., 1994. Crustal structures of the Ligurian, Tyrrhenian and Ionian seas and adjacent onshore areas interpreted from wide-angle seismic profiles. Boll. Geofis. Teor. Appl. 36 (141–144), 5–19.

Serpelloni, E., Anzidei, M., Baldi, P., Casula, G., Galvani, A., 2005. Crustal Velocity and Strain-Rate Fields in Italy and Surrounding Regions: New Results from the Analysis of.

Speranza, F., Hernandez-Moreno, C., Avellone, G., Gasparo Morticelli, M., Agate, M., Sulli, A., Di Stefano, E., 2018. Understanding paleomagnetic rotations in Sicily: Thrust versus strike-slip tectonics. Tectonics 37 (4), 1138–1158.

Stampfli, G.M., 2005. Plate Tectonics of the Apulia-Adria Microcontinents, CROP PROJECT: Deep seismic exploration of the Central Mediterranean and Italy, chapter 33, pp. 747–765.

Stampfli, G., Borel, G., 2002. A plate tectonic model for the Paleozoic and Mesozoic constrained by dynamic plate boundaries and restored synthetic oceanic isochrons. Earth Planet. Sci. Lett. 196, 17–33. https://doi.org/10.1016/S0012-821X (01)00588- X.

Stampfli, G.M., Borel, G.D., Cavazza, W., Mosar, J., Ziegler, P.A., 2001. Palaeotectonic and palaeogeographic evolution of the western Tethys and PeriTethyan domain (IGCP Project 369). Episodes 2001 (24), 222–228. https://doi.org/10.18814/epiiugs/2001/v24i4/001.

Sulli, A., Morticelli, M.G., Agate, M., Zizzo, E., 2021. Active north-vergent thrusting in the northern Sicily continental margin in the frame of the quaternary evolution of the Sicilian collisional system. Tectonophysics 802, 228717. ISSN 0040-1951. https://doi.org/10.1016/j.tecto.2021.228717.

Todaro, S., Sulli, A., Spatola, D., Micallef, A., Di Stefano, P., Basilone, G., 2021. Depositional mechanism of the upper Pliocene-Pleistocene shelf-slope system of the western Malta Plateau (Sicily Channel). Sediment. Geol. 417 https://doi.org/10.1016/j.sedgeo.2021.105882, 2021, 105882, ISSN 0037–0738.

Tonielli, R., Innangi, S., Di Martino, G., Romagoli, C., 2019. New bathymetry of the Linosa volcanic complex from multibeam systems (Sicily Channel, Mediterranean Sea). J. Maps 15, 611–618. https://doi.org/10.1080/17445647.2019.1642807.

Torelli, L., Grasso, M., Mazzoldi, G., Peis, D., Gori, D., 1995. Cretaceous to Neogene structural evolution of the Lampedusa shelf (Pelagian Sea, Central Mediterranean). Terra Nova 7, 200–212.

Vail, P.R., 1987. Seismic stratigraphy interpretation procedures. In: Bally, A.W. (Ed.), Atlas of Seismic Stratigraphy, AAPG Studies in Geology, 1, pp. 1–10. No. 27.

Van Hinsbergen, D.J.J., Torsvik, T.H., Schmid, S.M., Matenco, L.C., Maffione, M., Vissers, R.L.M., Gürer, D., Spakman, W., 2020. Orogenic architecture of the Mediterranean region and kinematic reconstruction of its tectonic evolution since the Triassic. Gondwana Res. 81, 79–229. https://doi.org/10.1016/j.gr.2019.07.009.

Washington, H.S., 1909. Art. VIII. —the submarine eruptions of 1831 and 1891 near Pantelleria. Amer. J. Sci. 27 (158), 131–150. https://doi.org/10.2475/ajs.s4-27.158.